arXiv:2507.15825v1 [stat.ME] 21 Jul 2025

ACS: An interactive framework for conformal selection

Yu Gui*[1], Ying Jin*[1], Yash Nair*[2], and Zhimei Ren*[1]

[1]Department of Statistics and Data Science, University of Pennsylvania
[2]Department of Statistics, Stanford University

July 22, 2025

Abstract

This paper presents adaptive conformal selection (ACS), an interactive framework for model-free selection with guaranteed error control. Building on conformal selection (Jin and Candès, 2023b), ACS generalizes the approach to support human-in-the-loop adaptive data analysis. Under the ACS framework, we can partially reuse the data to boost the selection power, make decisions on the fly while exploring the data, and incorporate new information or preferences as they arise. The key to ACS is a carefully designed principle that controls the information available for decision making, allowing the data analyst to explore the data adaptively while maintaining rigorous control of the false discovery rate (FDR). Based on the ACS framework, we provide concrete selection algorithms for various goals, including model update/selection, diversified selection, and incorporating newly available labeled data. The effectiveness of ACS is demonstrated through extensive numerical simulations and real-data applications in large language model (LLM) deployment and drug discovery.

1 Introduction

We study the problem of identifying promising units from a potentially large pool of candidates—for example, selecting drug candidates with high binding affinity to a target from a space of chemical compounds (Huang, 2007; Lavecchia and Di Giovanni, 2013), choosing job candidates from a pool of applicants (Sajjadiani et al., 2019), or filtering trustworthy outputs from language models (Gui et al., 2024). This problem can be viewed as selecting units whose unknown labels (e.g., binding affinities) obey a desired property. To this end, powerful machine learning models have been developed to predict these unknown label based on observable features (e.g., chemical structure), enabling efficient shortlisting in place of costly manual evaluation. However, due to the inherent uncertainty in predictions from complex models, a central challenge is to control the errors in the selection process, ensuring that the selected candidates are indeed promising.

To address this challenge, Jin and Candès (2023b) proposed conformal selection (CS), a statistically rigorous framework for shortlisting promising candidates with the assistance of any prediction machine. Assuming access to a set of labeled data whose properties of interest are known (e.g., drug candidates with measured binding affinities), CS sets aside a portion of them (training data) to fit a prediction model; it then uses the remaining labeled data (calibration data) to determine which unlabeled data (test data) to select. Provided that the calibration and test data are exchangeable, CS guarantees control of the false discovery rate (FDR)—the expected fraction of the selected units whose unknown outcomes do not satisfy the property of interest. Such guarantees hold regardless of the prediction model and do not require any modeling assumptions of the data distribution, thereby providing robust and model-agnostic guarantees for the selection.

Despite its flexibility and robustness, a key limitation of CS is that it separates the model choice from the selection process. All the components—including the split of labeled data, the model fitting procedure, choice of the conformity score that determines the ordering in which the units are selected—must be fixed a priori. This requirement prevents any changes to the analysis plan after seeing the calibration and test data, which can often be too rigid in practice. To illustrate this point, we present two applications below where the need for adaptive analysis strategies naturally arises:

*Author names listed alphabetically.

(1) In virtual screening for drug discovery, CS is used to identify which drug candidates should advance to later stages of development. With a pre-specified conformity score (fitted on the training fold), it ranks the test (unlabeled) drug candidates by their scores and leverages the calibration (labeled) data to determine how many top-ranked test drugs to select. However, if adaptive analysis were permitted, a scientist could adjust the initial data split—for example, reallocating some calibration data to the training set if the model appears underfit due to insufficient training samples, or switching to a more data-efficient model class if the original choice performs poorly. This flexibility is especially valuable when labeled data from prior campaigns are scarce. Furthermore, instead of adhering to a fixed ranking determined by the pre-specified conformity score, the scientist may re-prioritize selection after evaluating some candidates, in order to improve the overall diversity or novelty of the selection set (Nair et al., 2025).

(2) In the context of large language model (LLM) reliability, CS has been instantiated to filter trustworthy outcomes from a foundation model (Gui et al., 2024), selecting qualified outputs for direct deployment in downstream tasks while routing others to human experts for review. This expert feedback may create new labeled data beyond what was initially available. A natural question arises: can we leverage the newly labeled test data—when it becomes available—to improve the model fitting without compromising the error control guarantee?

In both applications, the practitioner may want to update the analysis plan after inspecting the data for various purposes. However, it is unclear how to achieve this without violating the FDR control offered by CS. Motivated by this practical need, we aim to address the following question:

> *To what extent can we incorporate additional information and/or make data-driven decisions within CS in an adaptive fashion, while maintaining the error control?*

Answering this question is nontrivial, since arbitrary changes to the analysis plan may introduce the risk of double-dipping. In order to preserve error control, we design a framework that governs precisely what information the decision maker is allowed to use in their analysis at each timestep of the selection process.

1.1 Adaptive Conformal Selection

We propose *adaptive conformal selection (ACS)*, a new framework that extends CS to support interactive data analysis in the selection process while maintaining exact FDR control in finite samples. In a nutshell, ACS is a sequential procedure that iteratively refines the ordering of candidates until a stopping criterion is met, at which point all the top-ordered candidates are selected. This interactive approach enables flexible changes to the analysis plan—allowing practitioners to incorporate new data, update prediction models, and prioritize complicated metrics like diversity after partially inspecting the data.

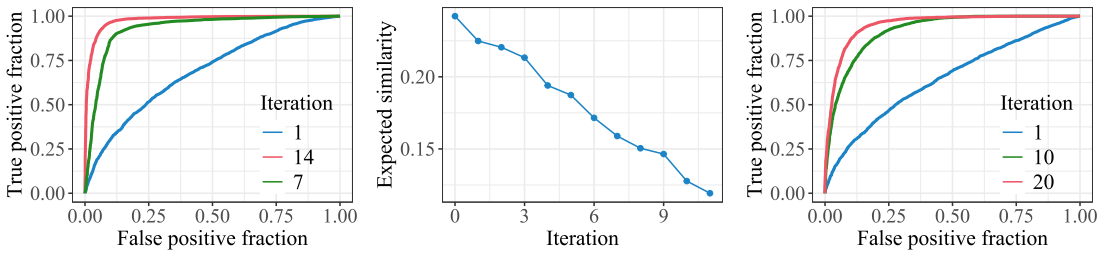
ACS begins by obtaining an initial predictive model with a subset of labeled data, which is then used to produce an initial ordering—from least to most promising—of both the (remaining) labeled and unlabeled candidates. The procedure then screens the least promising unit, reveals its label information, and examines the stopping criterion (i.e., whether an estimated false discovery proportion falls below the target level). If the criterion is not yet met, the newly screened data point can be used in any way to update the order of the remaining candidates. This process continues iteratively, with the candidate ranking updated at each step, until the stopping condition is satisfied. At that point, the remaining unlabeled candidates are selected as the final set.

As we shall show in the paper, ACS enjoys the same FDR control as CS. To achieve this, the only requirement in ACS is that the rule determining the ordering of the unscreened candidates is adapted to a carefully designed filtration. This filtration controls the information available to the analyst at each step, including all previously screened samples, among other information. As the screening proceeds, more information can be used to improve the ordering, which in turn leads to selections that are better aligned with the user's objectives. The adaptivity of ACS allows practitioners to pursue a range of goals that are not feasible under the static structure of CS. We summarize some of them below.

- **Model update and selection:** As more calibration data are screened, these labeled data can be incorporated to train a new model or conduct model selection. This improves the model's ability to correctly order the remaining candidates—by distinguishing promising from non-promising ones,

which ultimately leads to higher selection power. We demonstrate this phenomenon in panel (a) of Figure 1: in a simulation study, we track the fitted model's *receiver operating characteristic (ROC)* curve after the 1st, 7th, and 14th model updates. As the metric improves over updates, we observe a corresponding increase in selection power, as shown in Section 5.

- **Flexible preference:** Beyond optimizing power, the adaptivity of ACS allows the analyst to prioritize different considerations at different stages of the screening process. In drug discovery, a scientist may want to prioritize drug candidates with high binding affinity at the beginning, but as more candidates are screened, they may shift their preference toward drug candidates that are substantially different from the existing campaigns. With ACS, the analyst is free to update the scoring function—whether subjective or data-driven—to reflect evolving preferences, such as increasing the diversity of selected candidates. Panel (b) of Figure 1 plots a similarity measure among the remaining units over iterations. The decreasing similarity measure indicates increasing diversity.
- **Incorporating new labeled data:** In some applications, the screened (unselected) test candidates may be sent to a human expert for labeling (e.g., in the LLM filtering example introduced earlier). The newly labeled data can be integrated into later steps of the selection process, such as refining the fitted model (as demonstrated in Panel (c) of Figure 1). We will show in simulations and real-data applications in LLM deployment that this incorporation of new labels leads to improved selection power.



(a) Model update (b) Diversified selection (c) New labels

Figure 1: (a) The ROC curves of the (selected) prediction model at the 1^{st}, 7^{th}, and 14^{th} model updates; simulation details are provided in Section 5.3. (b) The expected similarity of the unscreened units with positive labels versus the screening rule updates; simulation details are provided in Section 5.4. (c) The ROC curves of the fitted random forest classifier at the 1^{st}, 10^{th}, and 20^{th} model updates; simulation details are in Section 5.5.

1.2 Organization of the paper

The rest of the paper is organized as follows. In Section 2, we introduce the problem setup and the notation used throughout the paper. We present the general framework of ACS in Section 3 and its instantiations in Section 4 for several specific desiderata introduced earlier. Section 5 presents simulations that demonstrate the performance of ACS; Sections 6 and 7 apply ACS to real-world applications in LLM deployment and drug discovery, respectively. The paper is concluded with a discussion in Section 8.

2 Preliminaries

2.1 Problem setup

Let $X \in \mathcal{X}$ denote the feature vector, and $Y \in \mathbb{R}$ the outcome of interest. Consider a set of labeled data $\mathcal{D}_{\text{lab}} = \{(X_i, Y_i)\}_{i=1}^n$, and test set $\mathcal{D}_{\text{test}} = \{X_{n+j}\}_{j=1}^m$, whose outcomes $\{Y_{n+j}\}_{j=1}^m$ are unobserved. We also denote $Z_i = (X_i, Y_i)$ for $i \in [n+m] := \{1, \ldots, n+m\}$ for notational convenience. For each unit $i \in [n+m]$, the property of interest is characterized by a set $\mathcal{C}_i$; we wish to pick out the test units with $Y_{n+j} \notin \mathcal{C}_{n+j}$. For example, when the goal is to detect the samples with $Y_{n+j} > 0$, we set $\mathcal{C}_{n+j} = (-\infty, 0]$. The only assumption we make on the data-generating process is as follows.

Assumption 1. *The property set $\mathcal{C}_i$ is observed for each $i \in [n+m]$, and $\{(X_i, Y_i, \mathcal{C}_i)\}_{i\in[n+m]}$ are jointly exchangeable across $i \in [n+m]$.*

Assumption 1 is quite mild and can be satisfied in many practical scenarios, for example, when the Z_i's are i.i.d. samples from some distribution, and the property sets $\mathcal{C}_i \equiv \mathcal{C}$ for some deterministic set $\mathcal{C}$ or $\mathcal{C}_i = c(X_i)$ for some deterministic function $c : \mathcal{X} \mapsto \mathbb{R}$. Following Jin and Candès (2023b), we approach this problem from a testing perspective: for each $j \in [m]$, consider the null hypothesis

$$H_{0,j} : Y_{n+j} \in \mathcal{C}_{n+j}.$$

When $H_{0,j}$ is rejected, we declare the j^{th} test sample to be interesting, and the selection problem can now be viewed as a multiple testing problem. We aim to design a selection algorithm $\mathcal{A}$ that takes as input $\mathcal{D}_{\text{lab}}$ and $\mathcal{D}_{\text{test}}$ and outputs a set of indices $\mathcal{S} \subseteq [m]$ that are declared as interesting. The FDR and power of $\mathcal{S}$ are defined as follows:

$$\text{FDR}(\mathcal{S}) = \mathbb{E}[\text{FDP}(\mathcal{S})], \qquad \text{FDP}(\mathcal{S}) = \frac{\sum_{j=1}^m \mathbb{1}\{j \in \mathcal{S}, Y_{n+j} \in \mathcal{C}_{n+j}\}}{|\mathcal{S}|},$$
$$\text{Power}(\mathcal{S}) = \mathbb{E}\left[\frac{\sum_{j=1}^m \mathbb{1}\{j \in \mathcal{S}, Y_{n+j} \notin \mathcal{C}_{n+j}\}}{\sum_{j=1}^m \mathbb{1}\{Y_{n+j} \notin \mathcal{C}_{n+j}\}}\right],$$

where we follow the convention that $0/0 = 0$ throughout the paper, and the expectation is taken over the randomness in $\mathcal{D}_{\text{lab}}$ and $\mathcal{D}_{\text{test}}$. We will use $\mathcal{H}_0 = \{j \in [m] : Y_{n+j} \in \mathcal{C}_{n+j}\}$ hereafter to denote the set of true null hypotheses (i.e., "uninteresting" samples), noting that $\mathcal{H}_0$ is random. Given a pre-specified FDR level $\alpha \in (0, 1)$, the goal is to select as many test samples as possible that are "interesting" while controlling the FDR at level α.

2.2 Background: conformal selection

The problem described above was first considered in Jin and Candès (2023b), with $\mathcal{C}_i$ in the form of $(-\infty, c_i]$ for some threshold $c_i \in \mathbb{R}$. They proposed the conformal selection (CS) procedure that builds upon the split conformal inference framework (Vovk et al., 2005; Papadopoulos et al., 2002; Lei et al., 2015). The CS procedure starts by splitting the training set $\mathcal{D}_{\text{lab}}$ into two parts: a model-fitting set $\mathcal{D}_{\text{train}}$ and a calibration set $\mathcal{D}_{\text{cal}}$. With slight abuse of the notation, we use $\mathcal{D}_{\text{train}}$, $\mathcal{D}_{\text{cal}}$ and $\mathcal{D}_{\text{test}}$ to denote either the samples or their indices when no confusion can arise from the context. Using $\mathcal{D}_{\text{train}}$, a predictive model $\widehat{f} : \mathcal{X} \mapsto \mathbb{R}$ is fitted; a conformal p-value (Vovk et al., 2005; Bates et al., 2023) is then computed for each test sample $j \in [m]$ by contrasting its predicted value $\widehat{f}(X_{n+j})$ with the predictions on the calibration set $\mathcal{D}_{\text{cal}}$:

$$p_j = \frac{1 + \sum_{i\in\mathcal{D}_{\text{cal}}} \mathbb{1}\{\widehat{f}(X_{n+j}) \geq \widehat{f}(X_i), Y_i \leq c_i\}}{|\mathcal{D}_{\text{cal}}| + 1}.$$

It can be proved that the conformal p-values are valid p-values, i.e., $\mathbb{P}(p_j \leq t, Y_{n+j} \leq c_{n+j}) \leq t$ for any $t \in [0, 1]$;[1] meanwhile, a small p_j suggests evidence against the null hypothesis $H_{0,j}$, indicating that the j^{th} test sample is likely to be interesting. The CS procedure finally selects the test samples by applying the Benjamini-Hochberg (BH) procedure (Benjamini and Hochberg, 1995) to the conformal p-values at level α. Jin and Candès (2023b) show that CS controls the FDR at level α under Assumption 1.

As mentioned in the introduction, CS is a one-shot procedure, requiring the analysis plan—e.g., the choice of prediction models, the type of scoring functions and the data usage—to be pre-determined before inspecting the data. Our work generalizes CS to enable adaptive data analysis while maintaining the FDR control. In our new proposal, one can iteratively improve the prediction model and perform data-driven model selection to boost the power of the selection procedure, and/or update the utility function based on (part of) the observed data adaptively.

2.3 Related work

This work relates to the line of research on model-free selection (Jin and Candès, 2023b), with applications in drug discovery (Jin and Candès, 2023a; Bai et al., 2024) and LLM deployment (Gui et al., 2024).

[1] There is another version of the conformal p-value involving a tie-breaking random variable $U_j \sim \text{Unif}[0, 1]$, which is not introduced here for simplicity. See Jin and Candès (2023b) for details and Gui et al. (2024) for the connection.

Recently, Bai and Jin (2024) extended CS to perform model selection in a data-driven manner aimed at power improvement. While this aligns with one of our key goals, the adaptivity of ACS offers additional flexibility: it enables the incorporation of expert preferences, supports complex objectives like diversity, and allows integration of new labeled data. Moreover, the techniques used in Bai and Jin (2024) are substantially different from ours. Other works have extended the model-free selection problem to various settings: (1) settings beyond the exchangeable data assumption (Jin and Candès, 2023a; Lee and Ren, 2025), (2) online selection (Xu and Ramdas, 2024; Huo et al., 2024), and (3) settings where the goal is to optimize metrics beyond the size of selection subject to constraints (Huo et al., 2024; Wu et al., 2024; Nair et al., 2025). The instantiation of ACS to promote diversity is most closely related to the third category—particularly Wu et al. (2024), who asymptotically optimize diversity metrics of the selection set, and Nair et al. (2025), who leveraged a similar martingale structure to ours that prunes the conformal selection set for enhanced diversity. In contrast to these approaches, ACS pursues diversity by adaptively updating the priority of unscreened candidates, rather than performing a global optimization over the selection set. Unlike Wu et al. (2024), ACS provides finite-sample FDR control without requiring any modeling assumptions. Compared with Nair et al. (2025), who always returns a subset of the original conformal selection set, ACS can—in some cases—improve both the diversity and the number of selected candidates by iteratively reordering candidates during the selection process.

Related to conformal selection, the literature on novelty detection with conformal p-values (Bates et al., 2023; Mary and Roquain, 2022; Marandon et al., 2024; Bashari et al., 2024; Liang et al., 2024; Lee et al., 2025a; Bashari et al., 2025; Lee et al., 2025b) concerns picking out from a pool of samples the outliers whose distribution differs from that of a reference set. While their setting is distinct from ours, our proposed method is also applicable to the novelty detection problem with slight modification.

Another related line of work is adaptive data analysis with statistical validity (Dwork et al., 2015; Tian and Taylor, 2018; Lei and Fithian, 2018; Weinstein et al., 2017; Lei et al., 2021; Balakrishnan and Wasserman, 2019; Duan et al., 2020; Yang et al., 2021; Chao and Fithian, 2021; Ren and Candès, 2023; Roy et al., 2025), where the research question is to design a protocol for human-in-the-loop data analysis that limits the amount of information accessible to the data analyst at different stages, so as to ensure the statistical validity in the presence of double-dipping. Our approach is similar in spirit, where the adaptivity and the statistical validity are both achieved by carefully controlling the information flow in the selection procedure. In particular, our design of protocol is inspired by that of Yang et al. (2021); they, however, focus on testing parametric hypotheses, while our hypotheses of interest are fully nonparametric.

3 Adaptive conformal selection

3.1 Warm-up: CS as a screening procedure

As a warm up, we first give an alternative interpretation of CS which builds the key intuition for ACS. To streamline the exposition, we set $\mathcal{C}_i \equiv (-\infty, 0]$ in this part.

In addition to the p-value perspective from Jin and Candès (2023b) introduced in Section 2.2, CS can also be interpreted as a sequential screening procedure (Mary and Roquain, 2022). Specifically, after fitting the prediction model on $\mathcal{D}_{\text{train}}$, each of the calibration and test samples is assigned a predicted value $\widehat{f}(X_i)$. CS then ranks the samples in ascending order of $\widehat{f}(X_i)$, from least to most promising. For notational convenience, let $k = |\mathcal{D}_{\text{train}}|$, and let π be a permutation of $\{k+1, \ldots, n+m\}$ such that $\widehat{f}(X_{\pi(k+1)}) \leq \ldots \leq \widehat{f}(X_{\pi(n+m)})$. CS proceeds by sequentially screening the samples in the order specified by π. At each step $\ell \geq k+1$, it computes the FDP estimate for the set of candidates ranked above $\pi(\ell)$, namely,

$$\widehat{\text{FDP}}(\ell) = \frac{m}{n-k+1} \cdot \frac{1 + \#\{j > \ell : \pi(j) \text{ is from } \mathcal{D}_{\text{cal}} \text{ and } Y_{\pi(j)} \leq 0\}}{\#\{j > \ell : \pi(j) \text{ is from } \mathcal{D}_{\text{test}}\}}.$$

The screening stops the first time $\widehat{\text{FDP}}(\ell) \leq \alpha$, and the remaining test samples are declared as interesting—this is the selection set $\mathcal{S}_{\text{CS}}$. See Figure 2 for an illustration of the screening process.

From this sequential screening perspective, the ordering π controls two aspects of the selection process: (1) the form of the final selection set, i.e., the relative ordering of the candidates, and (2) the stopping

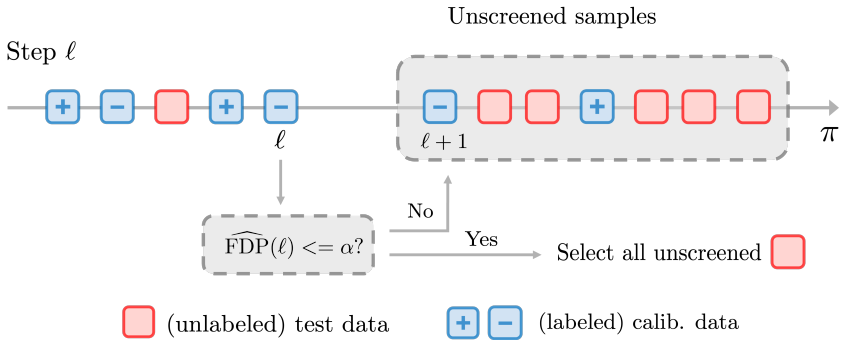


Figure 2: An illustration of the CS procedure as a sequential screening process, where the plus (resp. minus) signs correspond to interesting (resp. uninteresting) samples. The goal is to select positive test samples, and the calibration and test samples are ordered by their predicted values $\widehat{f}(X_i)$. At step ℓ, CS screens the sample corresponding to $\pi(\ell)$ if $\widehat{\mathrm{FDP}}(\ell)$ is above the target level α; otherwise it stops the screening and selects all the unscreened test samples.

time—i.e., how many top-ranked candidates are selected—determined by the estimated FDP at each step. Intuitively, a scientist seeking diversity among selected drug candidates should choose an ordering π that avoids clustering similar drugs in nearby ranks to reduce the risk of selecting a homogeneous set. A practitioner seeking high power should aim for an ordering π in which the test and positive calibration samples appear later in the screening (i.e., highly ranked in π) to decrease the FDP estimate.

To achieve these goals, it is highly desirable to adjust the ordering π after inspecting some of the calibration and test data. While such behavior is prevented in CS, we will show that ACS allows to update $\pi(\ell), \ldots, \pi(n+m)$ at every step ℓ using a rich set of information without compromising the FDR control, thereby enhancing the flexibility and efficacy of the selection procedure.

3.2 ACS: the general framework

As in CS, ACS sequentially screens the samples from the least promising to the most promising until a stopping criterion is met, then declaring the unscreened test samples as interesting. Importantly, the ordering of the unscreened samples can be updated adaptively with the newly available information revealed at each step. We formally describe the general procedure of ACS below.

Initialization. Before running ACS, we first randomly permute the order of all samples. Without loss of generality, let $[n+m]$ denote the indices of permuted samples, and $i \in [n+m]$ provides no information about whether the sample i belongs to the labeled set or not. For each $i \in [n+m]$, we define an indicator A_i such that $A_i = 0$ (resp. $A_i = 1$) if i corresponds to a labeled (resp. test) sample; we refer to A_i as the "membership information". Due to the permutation, one cannot tell whether X_i is from the labeled or test set without observing A_i. The goal of ACS is to adaptively determine a permutation π of $[n+m]$ that specifies the screening order, where the sample to be screened at step ℓ is $\pi(\ell)$. One may reserve a subset of size $k \geq 0$ among the labeled samples to initialize model training. Without loss of generality, we take $(\pi(1), \ldots, \pi(k))$ as a random subset of $\{i\colon A_i = 0\}$.

Adaptive screening. Next, for any $\ell \geq k$, we are to decide the next-to-screen sample $\pi(\ell+1)$ from the set of as-yet unscreened indices at time ℓ. We define the following quantities that will be useful for introducing the algorithm:

- The indices of already screened samples: $O_\ell := (\pi(1), \ldots, \pi(\ell))$;
- The index sets of non-null and null unscreened labeled samples:

$$N_\ell^+ = \{i \in [n+m] \backslash O_\ell : A_i = 0, Y_i \notin \mathcal{C}_i\},\ N_\ell^- = \{i \in [n+m] \backslash O_\ell : A_i = 0, Y_i \in \mathcal{C}_i\};$$

- The set of indices of unscreened test samples: $P_\ell = \{i \in [n+m] \backslash O_\ell \colon A_i = 1\}$;
- The index set of all the unscreened samples: $U_\ell = [n+m] \backslash O_\ell = N_\ell^+ \cup N_\ell^- \cup P_\ell$.

The only requirement that we impose on the screening order is that $\pi(\ell)$ is measurable with respect to the σ-algebra defined as follows:

$$\mathcal{F}_\ell = \sigma\left(O_\ell, |N_\ell^-|, |P_\ell|, \{(\tilde{Z}_i, A_i)\}_{i\in O_\ell \cup N_k^+}, \{X_i\}_{i\in U_\ell}\right). \tag{1}$$

Above, $|A|$ denotes the cardinality of a set A; $\tilde{Z}_i = Z_i$ if $A_i = 0$ and $\tilde{Z}_i = X_i$ otherwise. Note that in CS, $\{\pi(\ell)\}_{\ell>k}$ is determined purely by $\{\tilde{Z}_i, A_i\}_{i\in O_k}$ and $\{X_i\}_{i\in U_k}$, and therefore CS can be viewed as a special case of ACS.

The key restrictions imposed by $\mathcal{F}_\ell$ are as follows. First, the full data and membership information are revealed for $O_\ell \cup N_k^+$—that is, the previously screened (both labeled and test) samples and all the non-null labeled samples; these data can be used for training purposes in several applications of ACS, especially the labeled samples in them. Second, the term $\{X_i\}_{i\in U_\ell}$ means the covariates for the unscreened samples can be used without revealing their membership information; even though we do not know whether they belong to the test set, this can still be useful in several cases, e.g., checking the characteristics—such as diversity—of the unscreened candidates to gauge the screening preference. Finally, the only information we could use for the unscreened null labeled and test samples is their cardinality, i.e., $|N_\ell^-|$ and $|P_\ell|$. These constraints specify precisely the information available to the user in $\mathcal{F}_\ell$. We will see that this flexible and adaptive use of the sequentially revealed information in $\mathcal{F}_\ell$ enables us to use ACS for various distinct goals, described the next section.

Stopping rule. Finally, we specify how ACS stops the screening process and returns a final selection set. At each step $\ell \geq k$, we define an FDP estimate among the remaining unscreened test samples as

$$\widehat{\mathrm{FDP}}(\ell) = \frac{m}{n-k+1} \cdot \frac{1+|N_\ell^-|}{|P_\ell| \vee 1}, \tag{2}$$

where $a \vee b = \max(a, b)$. Intuitively, under the screening rule, the labeled and test null samples are exchangeable, so we would expect (roughly):

$$\frac{1+|N_\ell^-|}{n-k+1} \approx \frac{|P_\ell \cap \mathcal{H}_0|}{m},$$

which renders $\widehat{\mathrm{FDP}}(\ell)$ a reasonable estimate of the true FDP among the unscreened test samples. Whenever $\widehat{\mathrm{FDP}}(\ell) \leq \alpha$, we stop the screening process and declare the remaining test samples P_ℓ as selection. Otherwise, we continue to the next step and determine $\pi(\ell+1)$ using the above principle.

To summarize, ACS first assigns $\{\pi(i)\}_{i=1}^k$ as a random subset of those $A_i = 0$ for initialization; it then sequentially determines $\pi(\ell)$ for $\ell \geq k+1$, requiring that $\pi(\ell)$ is measurable with respect to $\mathcal{F}_{\ell-1}$. It returns the final selection set $\mathcal{S}_{\mathrm{ACS}} = P_T$, where we define the stopping time

$$T = \inf\{\ell \geq k : \widehat{\mathrm{FDP}}(\ell) \leq \alpha\},$$

with the FDP estimator defined in (2). The complete algorithm is summarized in Algorithm 1 and a graphical illustration is provided in Figure 3.

3.3 Theoretical guarantees

The following theorem establishes the FDR control of ACS.

Theorem 1. *Under Assumption 1, for any fixed $\alpha \in (0,1)$, the output of* ACS *applied at level α controls the FDR below α.*

We provide a sketch of the proof of Theorem 1 and defer the details to Appendix A.1. First, by the choice of T and the definition of the FDP estimator,

$$\mathrm{FDR}(\mathcal{S}_{\mathrm{ACS}}) = \mathbb{E}\left[\frac{|P_T \cap \mathcal{H}_0|}{|P_T|}\right] = \mathbb{E}\left[\widehat{\mathrm{FDP}}(T) \cdot \frac{n-k+1}{m} \frac{|P_T \cap \mathcal{H}_0|}{1+|N_T^-|}\right] \leq \alpha \frac{n-k+1}{m} \mathbb{E}\left[\frac{|P_T \cap \mathcal{H}_0|}{1+|N_T^-|}\right].$$

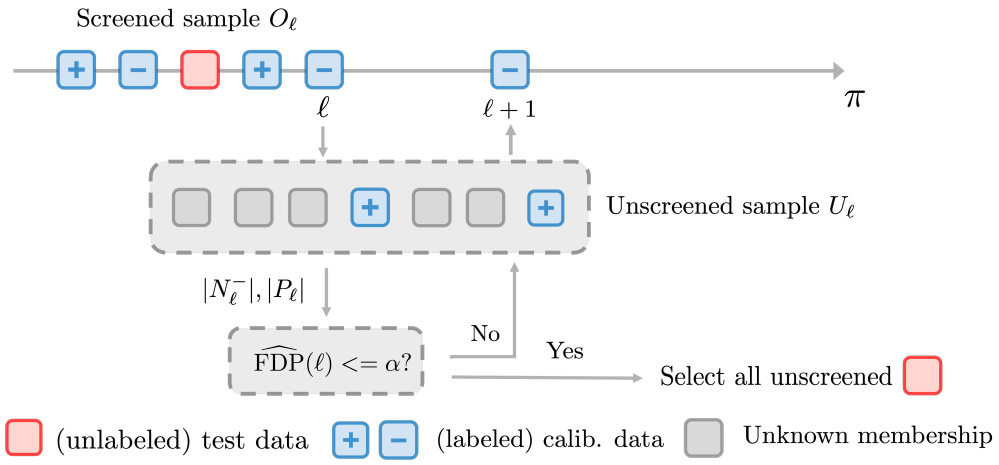


Figure 3: An illustration of the ACS procedure, where the plus (resp. minus) signs correspond to the interesting (resp. uninteresting) samples. The goal is to select interesting test samples. At step ℓ, if the FDP estimate $\widehat{\mathrm{FDP}}(\ell)$ is above the target level α, ACS determines the next sample to screen $\pi(\ell+1)$ from the unscreened candidates U_ℓ using the filtration $\mathcal{F}_\ell$ defined in (1); otherwise, it stops the screening and declares all the unscreened test samples as selection.

Algorithm 1 ACS: adaptive conformal selection

Input: Labeled samples $\{(X_i, Y_i)\}_{i\in[n]}$; test samples $\{X_{n+j}\}_{j\in[m]}$; target FDR level α; initial training sample size k.

Randomly permute the indices of all samples.
Initialize the screening order $\pi(i)$ for $i \in [k]$ by randomly choosing k samples with $A_i = 0$.
for $\ell = k, \ldots, n+m$ **do**
    Compute FDP estimate $\widehat{\mathrm{FDP}}(\ell)$ using (2).

    if $\widehat{\mathrm{FDP}}(\ell) \le \alpha$ **then**
        break ▷ Stop screening and declare the remaining test samples as interesting.
    end if
    Determine $\pi(\ell+1) \in U_\ell$ using $\mathcal{F}_\ell$ given in (1).
end for

Output: Rejection set P_ℓ^+.

At each step $\ell \ge k$, the elements in $P_\ell \cup N_\ell^-$ remain exchangeable despite the adaptive data analysis, since the update rule of ACS makes no use of their membership information. Using this fact, we prove that

$$M_\ell := \frac{|P_\ell \cap \mathcal{H}_0|}{1 + |N_\ell^-|}$$

is a super-martingale with respect to a filtration that is slightly richer than $\{\mathcal{F}_\ell\}_{\ell\ge k}$. The proof is completed by noting that T is a stopping time with respect to the same filtration and applying the optional stopping theorem. A similar martingale structure is used in Nair et al. (2025) to construct e-values for optimizing certain objectives—such as diversity—of the selected samples in conformal selection. However, the specific techniques differ significantly in the two works.

Remark 1. *As discussed earlier, ACS strictly generalizes the original framework of CS (Jin and Candès, 2023b): CS uses $\{Z_i\}_{i\in O_k}$ to train a prediction model $\widehat{g}$, which outputs scores measuring the likelihood of samples being interesting (non-null) and then uses the scores to determine the screening order. That is, $\{\pi(\ell)\}_{\ell>k}$ is purely determined by $\{(\tilde{Z}_i, A_i)\}_{i\in O_k}$ and $\{X_i\}_{i\in U_k}$, which is a subset of $\mathcal{F}_\ell$, for $\ell > k$.*

Remark 2 (Connection to existing adaptive multiple testing methods)**.** *Our interactive testing framework is closely related to the broader field of adaptive multiple testing. In particular, Lei and Fithian*

(2018); Yang et al. (2021) propose procedures that sequentially use partially revealed data to update rejection thresholds for each hypothesis, stopping once the estimated FDR falls below the target level. In both cases, the FDR control is achieved by constructing suitable martingales. As noted before, Yang et al. (2021) focus on testing parametric null hypotheses, while we consider fully nonparametric and random hypotheses. While the underlying principle is similar, our goals and implementation of this general idea differ significantly from those of prior works.

4 Instantiation of ACS

In this section, we present three instantiation of ACS, each serving distinct goals. Section 4.1 focuses on power improvement with adaptive model update and selection, Section 4.2 on diversifying the selection set, and Section 4.3 is about incorporating newly available labels for the screened-out units.

4.1 Boosting power

The screening order π plays a crucial role in the power of ACS. Intuitively, we would like to screen the least promising samples—those unlikely to be non-null test units—first, leaving the more promising ones towards the end: in this way, the FDP estimator stays lower and the sequential procedure has a higher chance of stopping earlier and selecting more interesting units. Naturally, this necessitates an accurate prediction model to discern null and non-null samples.

Model re-fitting. As the first instantiation of ACS, we propose to re-fit the prediction model periodically as more labeled samples enter the filtration $\mathcal{F}_\ell$. More specifically, at step $\ell \geq k$, we construct $\widehat{g}_\ell : \mathcal{X} \mapsto \mathbb{R}$ via

$$\widehat{g}_\ell = \mathcal{G}(Z_{\pi(1)}, \ldots, Z_{\pi(k)}, \tilde{Z}_{\pi(k+1)}, \ldots, \tilde{Z}_{\pi(\ell)}, X_{\pi(\ell+1)}, \ldots, X_{\pi(n+m)}),$$

recalling that $\tilde{Z}_i = Z_i$ if $A_i = 0$ and $\tilde{Z}_i = X_i$ otherwise; $\mathcal{G}$ is a model-fitting algorithm outputting a function that predicts the likelihood of a sample being interesting. The next-to-screen index $\pi_{\ell+1}$ is then determined by

$$\pi_{\ell+1} = \operatorname*{argmin}_{j \in U_\ell} \widehat{g}_\ell(X_j).$$

It is clear that $\pi_{\ell+1}$ is adapted to $\mathcal{F}_\ell$, and therefore this instantiation of ACS controls the FDR by Theorem 1. We note that in theory the *unscreened* non-null samples $\{Z_i\}_{i \in N_\ell^+}$ can also be used to update the model, i.e., allowing $\mathcal{G}$ to depend on $\{Z_i\}_{i \in N_\ell^+}$. However, we do not pursue this strategy here, as empirically we do not observe it to significantly improve the power.

The model-fitting algorithm $\mathcal{G}$ can, in principle, be any machine learning algorithm. Jin and Candès (2023b) shows that the choice of score maximizing the asymptotic power under FDR constraints should be a monotone function of $\mathbb{P}(Y \notin \mathcal{C} \,|\, X)$, i.e., the conditional probability of a sample being interesting given the covariates. Guided by this result, we suggest fitting a classification model for $\mathbb{1}\{Y \notin \mathcal{C}\}$ over X on the data $\{Z_i\}_{i=1}^k \cup \{Z_{\pi(i)} : A_{\pi(i)} = 0, k+1 \leq i \leq \ell\}$, i.e., all the labeled samples that have been screened at step ℓ; then, we set $\widehat{g}_\ell(x)$ to be the predicted probability of $Y \notin \mathcal{C}$ for x. As the screening procedure proceeds, more calibration samples can be used to fit the model, thereby improving its prediction accuracy (as visualized in panel (a) of Figure 1 in the introduction), the ordering of the remaining units, and ultimately the power of the selection procedure.

Adaptive model selection. Our adaptive framework also supports data-driven model selection while preserving FDR control. Suppose we have candidate models $\mathcal{G}_1, \ldots, \mathcal{G}_H$. At step $\ell \geq k$, we may want to pick the best model among the candidates to guide the subsequent screening order. We propose a cross-validation-based procedure for model selection using the available information.

Let $\mathcal{D}_{\text{lab},\ell} := \{Z_i\}_{i=1}^k \cup \{Z_{\pi(i)} : A_{\pi(i)} = 0, k+1 \leq i \leq \ell\}$ denote all the screened labeled samples available at timestep ℓ. We randomly split $\mathcal{D}_{\text{lab},\ell}$ into K non-overlapping folds $\{\mathcal{D}_{\text{lab},\ell}^{(k)}\}_{k=1}^K$. Then, for each $k \in [K]$ and each $h \in [H]$, we obtain a selection set $\mathcal{S}_{h,k}$ by running the CS procedure with prediction model $\mathcal{G}_h$, treating $\mathcal{D}_{\text{lab},\ell}^{(-k)} := \mathcal{D}_{\text{lab},\ell} \backslash \mathcal{D}_{\text{lab},\ell}^{(k)}$ as the training set, $\mathcal{D}_{\text{lab},\ell}^{(k)}$ as the calibration set, and $\{X_i\}_{i \in U_\ell}$

as the test set. We then measure the performance of $\mathcal{G}_h$ by the average number of selections across the K folds, and select the best model as

$$\widehat{h}_\ell = \underset{h\in[H]}{\operatorname{argmax}} \frac{1}{K}\sum_{k\in[K]}|\mathcal{S}_{h,k}|.$$

Since CS is agnostic to the order of the test samples, one can check that the proposed model selection procedure is adapted to $\mathcal{F}_\ell$, thereby preserving FDR control by Theorem 1.

Model update frequency. In principle, the prediction model can be updated at every step as new information in $\mathcal{F}_\ell$ becomes available. However, this may be computationally expensive in practice. To balance computational cost and power improvement, one may the model every L steps, where the hyperparameter L can be chosen by the user based on their computational constraints.

4.2 Diversifying selection

In many applications, in addition to maximizing the power, it is desired to optimize the diversity of the selection set. In drug discovery, scientists may want to include drug candidates with distinct action mechanisms in the selection set. However, with a pre-specified score function, CS is highly likely to select many similar drugs with similar predicted values. Since the diversity depends on the composition of the entire selection set, diversifying conformal selection while preserving FDR control proves challenging. Existing works either resort to asymptotic analysis assuming accurate modeling (Huo et al., 2024) or require complex recursive optimization (Nair et al., 2025).

Our second instantiation presents a novel solution to this problem by dynamically promoting "more diverse" drugs based on available information in the process. The intuition is that as more drugs are screened, the information in $\mathcal{F}_\ell$ allows the analyst to inspect the diversity of the unscreened drugs and design strategies to promote less-visited ones. For instance, if many test drugs in one region have been screened (i.e., excluded from the selection set), the remaining drugs in this region may be favored in subsequent rankings, so that they have a higher chance to be selected.

Formally, we introduce a function $\theta : \mathcal{X}\times\mathcal{X}\mapsto\mathbb{R}$ to measure the similarity between two units. Common choices for θ include the *radial basis function (RBF)* kernel $\theta(x_i,x_j)=\exp(-\|x_i-x_j\|^2/\sigma_0^2)$ for some user-specified $\sigma_0>0$, or the *cosine similarity* $\theta(x_i,x_j)=\frac{x_i^\top x_j}{\|x_i\|\|x_j\|}$; see Yang et al. (2015); Zhong et al. (2017); Wu et al. (2024); Huo et al. (2024) for more details. Given θ, the diversity of a set of units $\mathcal{S}\subseteq[m]$ can be measured by the *expected similarity (ES)*:

$$\mathrm{ES}_\theta(\mathcal{S}) = \mathbb{E}\left[\frac{\sum_{1\le i<j\le m}\mathbb{1}\{i\in\mathcal{S},j\in\mathcal{S}\}\delta_i\delta_j\cdot\theta(X_{n+i},X_{n+j})}{\sum_{1\le i<j\le m}\mathbb{1}\{i\in\mathcal{S},j\in\mathcal{S}\}\delta_i\delta_j}\right],$$

where $\delta_i=\mathbb{1}\{Y_{n+i}\notin\mathcal{C}_{n+i}\}$, for $i\in[m]$. By definition, $\mathrm{ES}_\theta(\mathcal{S})$ measures the similarity of the correctly selected units in $\mathcal{S}$, and is smaller when the selected units are more diverse. Roughly speaking, we aim to optimize a weighted combination of the power and diversity of a selection set $\mathcal{S}\subseteq[m]$:

$$L(\mathcal{S};\lambda) = (1-\lambda)\cdot\mathrm{Power}(\mathcal{S}) - \lambda\cdot\mathrm{ES}_\theta(\mathcal{S}),$$

where $\lambda\in[0,1]$ is a user-specified parameter that balances the two objectives. When $\lambda=0$, we recover the original power-based selection, and when $\lambda=1$, the selection is solely based on diversity.

4.2.1 Diversity-aware ordering

In order to connect the ordering strategy in ACS with the objective function $L(\mathcal{S};\lambda)$, our approach produces a score for each test unit, which will be used in the ordering (Xie et al., 2024). To be specific, at step $\ell\ge k$, we aim to select from a pool of $\tilde{n}:=n+m-\ell$ test units given their features. To simplify the notation, we use $X_1,\ldots,X_{\tilde{n}}$ to denote these test features in this section, when no confusion can arise given the context.

We assign each sample i a score of the form $(1-\lambda)\widehat{\delta}_i+\lambda\widehat{\xi}_i$, where $\widehat{\delta}_i$ promotes high power, and $\widehat{\xi}_i$ promotes greater diversity. While the specific choice of $\widehat{\delta}_i$ and $\widehat{\xi}_i$ are flexible, we introduce below a general principle for building effective scores. Specifically, we set $\widehat{\delta}_i$ as the current estimate of $\mathbb{P}(Y_i\notin\mathcal{C}_i\,|\,X_i)$,

$\forall i \in [\tilde{n}]$, obtained with the available information at step ℓ. For the diversity part, we use a function $\xi : \mathcal{X} \mapsto [0,1]$ to represent the "probability" of being selected, which will be optimized for diversity subject to FDR control. Consider the population objective with FDR control constraints:

$$\begin{aligned} \min_{\xi:\mathcal{X}\mapsto[0,1]} \ & \frac{\mathbb{E}\big[\xi(X_1)\xi(X_2)\delta_1\delta_2 \cdot \theta(X_1,X_2)\big]}{\mathbb{E}\big[\xi(X_1)\xi(X_2)\delta_1\delta_2\big]} \\ \text{s.t.} \ & \frac{\mathbb{E}\big[\xi(X_1)(1-\delta_1)\big]}{\mathbb{E}[\xi(X_1)]} \le \alpha, \end{aligned} \tag{3}$$

where $Z_i = (X_i, Y_i)$ for $i \in \{1,2\}$ are i.i.d. samples from the joint distribution of (X,Y). Intuitively, in (3), the objective function approximates ES_θ when the probability of selecting a unit X_i is given by $\xi(X_i)$, while the constraint is a proxy for the FDR control. A similar relaxation strategy is adopted by Huo et al. (2024). We note that the FDR constraint in (3) is optional, since the FDR control guarantee of the final selection set will always be guaranteed by the ACS framework regardless of the constraint.

The empirical version of the population-level problem (3) can be solved using off-the-shelf optimization algorithms if desired. In the next, we introduce a special relaxation which admits a closed-form solution. To be specific, we compute $\{\xi_i\}_{i=1}^{\tilde{n}}$ by solving the following relaxed empirical version of (3):

$$\begin{aligned} \min_{\{\xi_i\}_{i=1}^{\tilde{n}}} \ & \frac{\sum_{i,j=1}^{\tilde{n}} \xi_i\xi_j\widehat{\delta}_i\widehat{\delta}_j \cdot \theta(X_i,X_j)}{\sum_{i,j=1}^{\tilde{n}} \xi_i\xi_j\widehat{\delta}_i\widehat{\delta}_j} \\ \text{s.t.} \ & \frac{\sum_{i=1}^{\tilde{n}} \xi_i(1-\widehat{\delta}_i)}{\sum_{i=1}^{\tilde{n}} \xi_i} = \alpha, \\ & \xi^\top\widehat{\delta} > 0. \end{aligned} \tag{4}$$

Note that in (4), we relax the range constraint $\xi \in [0,1]$ to $\xi^\top\widehat{\delta} > 0$, as both the objective and the constraint are invariant to the scaling of ξ and only the relative importance of units is of interest in the ACS framework; the estimated FDR is forced to be α, since using up the budget of false discoveries only increases the power. Such a relaxation leads to a closed-form solution, stated in the proposition below. Its proof is deferred to Appendix A.2.

Proposition 1. *Let $\Theta \in \mathbb{R}^{\tilde{n}\times\tilde{n}}$ be the matrix with (i,j)-the entry $\widehat{\delta}_i\widehat{\delta}_j\theta(X_i,X_j)$ and let $\widehat{\delta} = (\widehat{\delta}_1,\ldots,\widehat{\delta}_{\tilde{n}})$. Assume that Θ is positive definite. Define $a = \widehat{\delta}^\top\Theta^{-1}\mathbf{1}_{\tilde{n}}$, $b = \widehat{\delta}^\top\Theta^{-1}\widehat{\delta}$, and $c = \mathbf{1}_{\tilde{n}}^\top\Theta^{-1}\mathbf{1}_{\tilde{n}}$. The optimal solution to (4) is given by*

$$\xi^* \propto \xi_0 := \Big(\frac{b}{1-\alpha} - a\Big)\Theta^{-1}\mathbf{1}_{\tilde{n}} - \Big(\frac{a}{1-\alpha} - c\Big)\Theta^{-1}\widehat{\delta}.$$

In our implementation, we threshold ξ_0 at 0 and normalize it to be bounded in $[0,1]$ to obtain the "working" selection rule: $\xi_{\text{work}} = \max(0,\xi^*)/\max(\xi^*)$. The order of the remaining units is determined by $\lambda\xi_{\text{work}} + (1-\lambda)\widehat{\delta}$, where $\lambda \in [0,1]$ is the user-specified parameter that balances the power and diversity; we discuss the specific choices of λ in our experiments in Section 5.4.

It is straightforward to check that the ordering strategy is adapted to the filtration $\mathcal{F}_\ell$, and therefore the resulting selection procedure still has its FDR controlled below α due to Theorem 1.

4.3 Incorporating new labels

Our last instantiation concerns incorporating newly available labels from the screened samples. In the LLM deployment example, the test units that are ruled out by the selection process may be sent to human annotators for labeling. Once available, these labels can be integrated into ACS to improve the prediction model.

Formally, at step $\ell \ge k$, assume that we additionally have access to the label Y_i for $i \in \mathcal{L}_\ell \subseteq \{j \in O_\ell : A_j = 1\}$. We can then train the prediction model $\widehat{g}_\ell$ via

$$\widehat{g}_\ell = \mathcal{G}(Z_{\pi(1)},\ldots,Z_{\pi(k)},\tilde{Z}_{\pi(k+1)},\ldots,\tilde{Z}_{\pi(\ell)},X_{\pi(\ell+1)},\ldots,X_{\pi(n+m)}),$$

where $\tilde{Z}_i = Z_i$ if $A_i = 0$ or $i \in \mathcal{L}_\ell$, and $\tilde{Z}_i = X_i$ otherwise. As before, the unit to be screened at step $\ell + 1$ is chosen via

$$\pi_{\ell+1} = \operatorname*{argmin}_{i \in U_\ell} \widehat{g}_\ell(X_i).$$

Although $\widehat{\pi}_\ell$ is no longer adapted to the filtration $\mathcal{F}_\ell$ as defined in (1), it is adapted to a slightly richer filtration—which incorporates the new label information as it becomes available—for which the proof of Theorem 1 still goes through. This is an implication of the proof of Theorem 1; see Appendix A.1.

5 Numerical simulations

This section contains simulation studies to evaluate the performance of ACS in various settings. In Section 5.1 we lay out the simulation setups. Section 5.2 compares ACS and CS with various base learners, and Section 5.3 shows the performance of ACS with adaptive model selection; Section 5.5 and 5.4 demonstrate the performance of ACS for diversity-oriented selection and incorporating new labels, respectively.

5.1 Simulation setup

Our simulation setups follow those in Jin and Candès (2023b). The covariates X_i are i.i.d. sampled from $\mathrm{Unif}[-1,1]^{20}$ and the response Y_i is generated from the model: $Y_i = \mu(X_i) + \varepsilon_i$, where $\mu(x)$ is the true regression function, and ε_i's are independent Gaussian noise terms. Throughout this section, the true regression function is set to be

$$\mu(x) = 4\mathbb{1}\{x_1 x_2 > 0\} \cdot \max\{x_4, 0.5\} + 4\mathbb{1}\{x_1 x_2 \le 0\} \cdot \min\{x_4, -0.5\}.$$

The noise term ε_i is i.i.d. from $\mathcal{N}(0, \sigma^2)$, with $\sigma \in \{0.03, 0.06, \ldots, 0.15\}$ unless otherwise specified. Appendix C provides additional simulation results for other choices of $\mu(x)$ and the noise distribution.

We take the property set $\mathcal{C}_i = (-\infty, 0]$, for $i \in [n+m]$. That is, the goal is to select units with $Y_{n+j} > 0$. The number of test units is fixed to be $m = 100$, except for the simulations in Section 5.4, where $m = 200$. The number of labeled units is $2n$ for both CS and ACS, with $n \in \{200, 500, 1000\}$. For CS, n units are used for training and the remaining n for calibration; in ACS, we similarly set $k = n$ to ensure a fair comparison. We consider gradient boosting (GB), random forest (RF), and support vector machine (SVM) as the model fitting function $\mathcal{G}$, implemented via the `scikit-learn` Python package (Pedregosa et al., 2011), without hyperparameter tuning. The target FDR level is set as $\alpha = 0.1$.

For each setting, we repeat the simulation $N = 1{,}000$ times, and report the average power, FDR, and ES. In specific, letting $\mathcal{S}^{(i)}$ denote the selection set in the i^{th} simulation and $Y^{(i)}_{n+j}$ the j^{th} test unit in the i^{th} simulation, we compute the following quantities:

$$\widehat{\text{Power}} = \frac{1}{N}\sum_{i=1}^{N} \frac{\sum_{j=1}^{m} \mathbb{1}\{Y^{(i)}_{n+j} > 0, j \in \mathcal{S}^{(i)}\}}{\sum_{j=1}^{m} \mathbb{1}\{Y^{(i)}_{n+j} > 0\}},$$

$$\widehat{\text{FDR}} = \frac{1}{N}\sum_{i=1}^{N} \frac{\sum_{j=1}^{m} \mathbb{1}\{Y^{(i)}_{n+j} \le 0, j \in \mathcal{S}^{(i)}\}}{|\mathcal{S}^{(i)}|},$$

$$\widehat{\text{ES}} = \frac{1}{|\mathcal{N}_2|}\sum_{i \in \mathcal{N}_2} \frac{\sum_{1 \le j < k \le m} \mathbb{1}\{j \in \mathcal{S}^{(i)}, k \in \mathcal{S}^{(i)}\} \cdot \mathbb{1}\{Y^{(i)}_{n+j} > 0, Y^{(i)}_{n+k} > 0\} \cdot \theta(X^{(i)}_{n+j}, X^{(i)}_{n+k})}{\sum_{1 \le j < k \le m} \mathbb{1}\{j \in \mathcal{S}^{(i)}, k \in \mathcal{S}^{(i)}\} \cdot \mathbb{1}\{Y^{(i)}_{n+j} > 0, Y^{(i)}_{n+k} > 0\}},$$

where $\mathcal{N}_2$ is the set of simulations with at least two units selected.

5.2 ACS with model-refitting: individual base models

We first compare ACS with CS under different fixed base models $\mathcal{G}$, following the procedure in the "Model re-fitting" part of Section 4.1. In this case, we re-fit the prediction model—within a fixed model class—every $L = 10$ steps with all labeled samples that have been screened up to step ℓ; the ordering of

the unscreened samples is then determined by the most recently re-fitted model and remains fixed until the next model update.

We fix $\mathcal{G} \in \{\text{GB}, \text{RF}, \text{SVR}\}$ and $n \in \{200, 500, 1000\}$. Figure 4 shows the realized power and FDR of CS and ACS. Both methods achieve the target FDR level $\alpha = 0.1$ in all settings, confirming the theoretical results. For any choice of $\mathcal{G}$ and any n, ACS achieves higher power than CS, and the improvement is more significant when n is smaller and/or the signal-to-noise ratio is lower. The power gain of ACS over CS in such cases is primarily due to the increased number of labeled data for model fitting, which leads to a more accurate prediction model and hence a better ordering of the units.

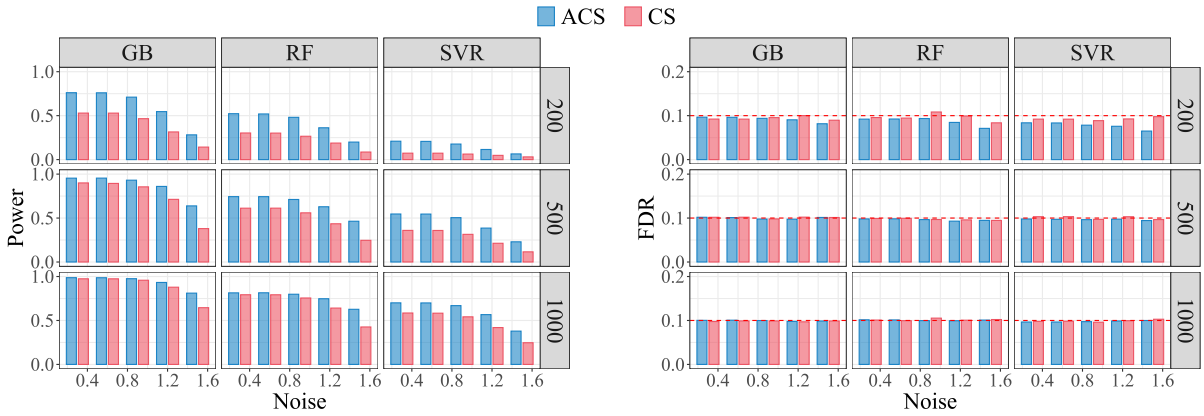


Figure 4: Realized power (left) and FDR (right) of ACS and CS for various noise levels σ. Each column corresponds to one of three fixed base models: gradient boosting (GB), random forest (RF), and support vector machine (SVR). Each row corresponds to one sample size $n \in \{200, 500, 1000\}$. The target FDR level is $\alpha = 0.1$ and the results are averaged over 1,000 independent runs.

5.3 ACS with model-refitting: adaptive model selection

Under the same setup of Section 5.2, we evaluate the performance of ACS using the procedure described in the "Adaptive model selection" part of Section 4.1. In our implementation, at every $L = 20$ steps, ACS adaptively chooses from the candidate models $\{\text{GB}, \text{RF}, \text{SVR}\}$ as the working model, and re-fit the chosen model with all the labeled data screened up to the currents step. The ordering of the unscreened samples is then determined by the most recently updated model and remains fixed until the next update. To study the impact of incorporating additional labeled samples into the filtration, we also implement a heuristic approach that selects the model based on the estimated mean squared error (MSE) of the fitted model computed on the training data—that is, both model fitting and MSE computation are performed using $\mathcal{D}_{\text{train}}$. We refer to this approach as the "naive" method, which allows for model selection (on the training data) but does not leverage additional labeled data.

Figure 5 plots the realized power and FDR curves of ACS with adaptive model selection, the naive method, CS-SVR, CS-GB, and CS-RF. It can be observed that ACS with adaptive model selection outperforms all the CS-based methods—as well as the naive approach—in terms of power, while maintaining the target FDR level.

As in the previous case, the power gain of ACS over CS is more significant when n is smaller and/or the signal-to-noise ratio is lower. With adaptive model selection, ACS can effectively leverage the strengths of different base models and adapt to the data structure without compromising the FDR control. The improvement in power is a combination of choosing the best model for the data and the increased number of labeled data for model fitting.

5.4 Diversified selection

We now study the performance of ACS with diversified selection, as introduced in Section 5.4. In this experiment, we take the number of test samples to be $m = 200$ and $n \in \{500, 1000\}$; the base model is set to be gradient boosting (GB), and the noise level ranges in $\{0.3, 0.6, \ldots, 3\}$. For the diversity measure θ, we adopt the the RBF kernel with $\sigma_0 = 5$. The other setups are the same as in the previous sections.

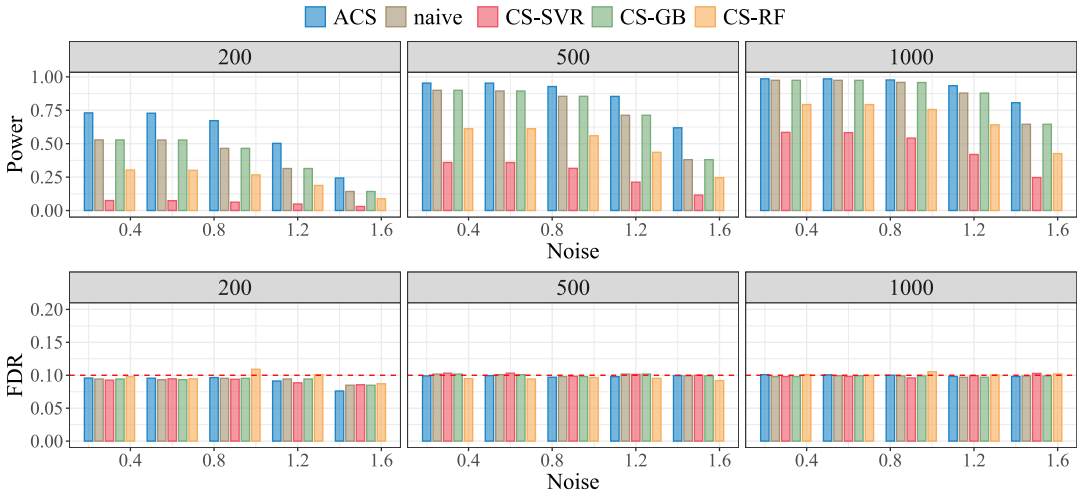


Figure 5: Realized power (top) and FDR (bottom) of ACS with adaptive model selection, the naive method, CS-SVR, CS-RF, and CS-GB, as a function of the noise level σ. The target FDR level is $\alpha = 0.1$ and the results are averaged over 1,000 independent simulations.

For ACS, we implement the diversity-aware version, where the ordering at each step $\ell \geq k$ is decided by the "mixture" score proposed in Section 5.4:

$$\pi_{\ell+1} = \underset{j \in U_\ell}{\operatorname{argmin}} \ \lambda \xi_{\text{work}_j} + (1-\lambda)\widehat{\delta}_j,$$

where $\lambda \in [0,1]$ is the user-defined parameter that controls the relative weight of diversity over power. In this experiment, we set $\lambda = 0.3$; results for other choices of λ can be found in Appendix C, and panel (b) of Figure 1 corresponds to $\lambda = 1$. The score is updated every $L = 10$ steps. We compare the performance of diversity-aware ACS with the power-oriented ACS (with $\lambda = 0$) and CS.

Figure 6 plots the ES-Power curves for the three methods. The realized ES of diversity-aware ACS is substantially lower than the other two methods at each power level, demonstrating the overall improvement in diversity. Figure 7 shows the realized power and FDR of the three methods at various noise levels. As expected, the FDR of all methods is controlled at the target level $\alpha = 0.1$; the power of diversity-aware ACS is a bit lower than that of ACS, which is also reasonable since it refrains from making a selection that is similar to the other selected. Perhaps a bit surprisingly though, diversity-aware ACS achieves a higher power than CS, while promising a more diversified selection. This shows that—through iteratively re-fitting the model and updating the scoring function—ACS finds better orderings of the unscreened samples that not only improve the power but also better discern the null and non-null samples.

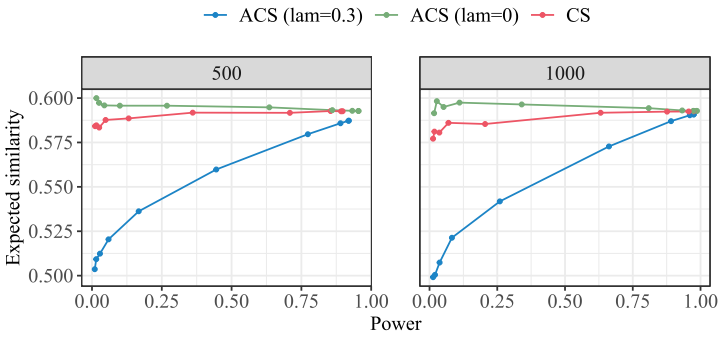


Figure 6: $\widehat{\text{ES}}$ as a function of $\widehat{\text{Power}}$ for diversity-aware ACS with $\lambda = 0.3$, ACS, and CS. The noise level σ is varied in $\{0.3, 0.6, \ldots, 3\}$ and the results are averaged over 1,000 independent simulations.

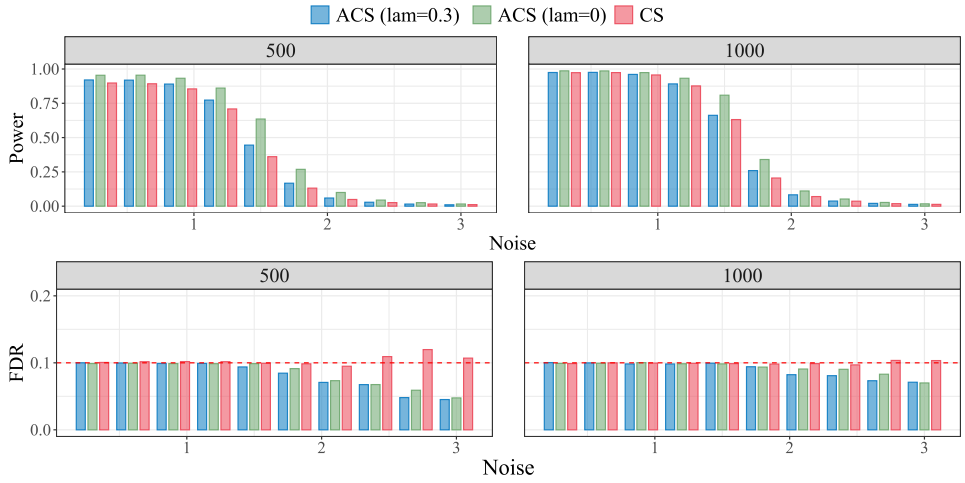


Figure 7: Realized power (left) and FDR (right) as a function of the noise level σ for diversity-aware ACS with $\lambda = 0.3$, ACS, and CS. The other details are the same as in Figure 6.

5.5 Incorporating new labels

We now study the procedure in Section 4.3, in a setting where the true labels of the test units become available *after* they are screened (i.e., knowing that they are not selected). Here, ACS leverages the new labels in re-fitting the model for every $L = 10$ steps—that is, the model is fitted with $\{(Z_i, A_i)\}_{i \in O_\ell}$. Figure 8 shows the realized power and FDR of ACS that incorporates the new labels (referred to as ACS-aug), as well as those of the original ACS and CS.

ACS-aug further improves the power of ACS, as more labeled data are available for model fitting. The FDR control is preserved in all settings, and the improvement in power is, as before, more significant when n is smaller and/or the signal-to-noise ratio is lower.

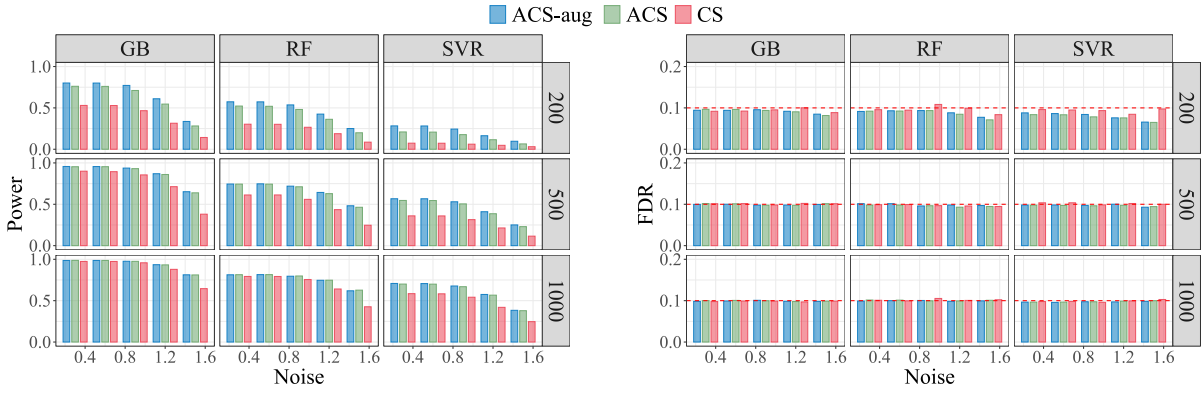


Figure 8: Power (left) and FDR (right) of ACS with new labels (ACS-aug), ACS without new labels (ACS), and CS as a function of the noise level σ. The simulation results correspond to the setting in Section 5.5, where the true labels of the test units are revealed after being screened. The target FDR level is $\alpha = 0.1$ and the results are averaged over 1,000 independent simulations.

6 Real data application: LLM deployment

In this section, we demonstrate the application of ACS to selective deployment of foundation model outputs, following the setup of Gui et al. (2024). Here, we view a prompt-output pair as a unit, and seek to select a subset of prompts whose outputs are aligned with human evaluations. Two specific tasks are considered: question answering and chest X-ray (CXR) report generation.

Background. In both examples, we let E_i denote the expert (gold-standard) input corresponding to a prompt X_i. For example, if X_i is a question, E_i is the true answer, and if X_i is a medical image, E_i is the radiology report written by a medical expert. The E_i's are only available in the labeled dataset.

Given a foundation model $f\colon \mathcal{X} \to \mathcal{Y}$ that generates an output $f(X) \in \mathcal{Y}$ given an input prompt $X \in \mathcal{X}$, we assume access to an evaluation function $\mathcal{A} : \mathcal{Y} \times \mathcal{Y} \mapsto \{0, 1\}$ that takes the foundation model output $f(X_i)$ and the expert input E_i as inputs, and outputs a binary alignment score $Y_i = \mathcal{A}(f(X_i), E_i) \in \{0, 1\}$. The specific form of the evaluation function $\mathcal{A}$ will be specified in each task. The alignment score $Y_i = 1$ indicates that the output $f(X_i)$ is aligned with the expert input E_i, while $Y_i = 0$ indicates misalignment. Since the E_i's are only available in $\mathcal{D}_{\text{lab}}$, we only observe the alignment scores Y_i in $\mathcal{D}_{\text{lab}}$; the goal is to select a subset of the test units with $Y_{n+j} = 1$. In other words, the null hypothesis of interest takes the form $\mathcal{H}_{0,j} : Y_j \in \mathcal{C}_j$ with $\mathcal{C}_j = \{0\}$.

Experimental setup. We fix the size of the test set at $m = |\mathcal{D}_{\text{test}}| = 1000$ and the set of labeled samples (those with expert output) is of size N; the latter is further partitioned into three subsets $\mathcal{D}_{\text{train}} \cup \mathcal{D}_{\text{tune}} \cup \mathcal{D}$. Throughout, we fix $|\mathcal{D}_{\text{train}}|/N = 0.1$, $|\mathcal{D}_{\text{tune}}|/N = 0.2$, and vary N in $\{100, 500, 1000\}$.

Following Gui et al. (2024), to build the prediction model, we use $\mathcal{D}_{\text{tune}}$ for feature engineering, where we extract certain features from the foundation model outputs—such as self-evaluation likelihoods (Kadavath et al., 2022; Lin et al., 2023), input uncertainty scores (Kuhn et al., 2023; Lin et al., 2023), and output confidence scores (Lin et al., 2023; Gui et al., 2024)—as the covariates $\tilde{X}_i$. Based on the extracted covariates $\tilde{X}_i$, we fit the model for predicting the alignment scores Y_i using $\mathcal{D}_{\text{train}}$, with base classifiers including logistic regression (`logistic`), random forests (`RF`), and XGBoost (`XGBRF`). More details are deferred to Appendix D.1.

6.1 Experiments for question answering (QA) datasets

We begin with the question answering task, where we select question answers that are sufficiently close to the correct answers in two widely adopted datasets: a conversational question answering dataset **TriviaQA** (Joshi et al., 2017) and a closed-book reading comprehension dataset **CoQA** (Reddy et al., 2019). To investigate the performance across LLMs with different capabilities, we employ two LLMs (without finetuning) **OPT-13B** (Zhang et al., 2023) and **LLaMA-2-13B-chat** (Touvron et al., 2023) to generate an answer $f(X_i)$ given the input questions X_i.[2] The alignment score Y_i is chosen to be $\mathbf{1}\{\texttt{rouge-L}_i \geq 0.3\}$ following Kuhn et al. (2023); Lin et al. (2023); Gui et al. (2024), where the `rouge-L` score (Lin, 2004) measures the similarity between generated and correct answers based on the longest common subsequences.

ACS and ACS-aug with individual base models. Following the setup in Section 5.2, we implement both CS and ACS, fixing $\mathcal{G} \in \{\texttt{logistic}, \texttt{RF}, \texttt{XGBRF}\}$. Figure 9 presents results on the CoQA dataset with LLaMA-2-13B-chat as the base language model; results for OPT-13B and the TriviaQA dataset are deferred to Appendix D.1. As shown in the figures, both ACS and CS successfully control the FDR across all base classifiers. However, ACS consistently achieves substantially higher power, particularly at lower nominal FDR levels. The power advantage of ACS is especially pronounced when $N = 100$ and `XGBRF` is the base classifier, highlighting the power advantage of ACS in settings with limited samples and data-consuming predictive models.

We further consider the scenario in Section 5.5 where alignment scores are revealed after screening, in which case, the effective sample size keeps increasing and can be used for updating the prediction model in the ACS framework; we refer to this variant as ACS-aug. In our experiment, we fix the model class for ACS-aug, and retrain the model using all labeled, screened data every $L = 20$ steps. The results for ACS-aug, also shown in Figure 9, demonstrate further improvements in power—particularly in settings with a limited number of labeled samples (i.e., when N is small).

ACS with adaptive model selection. Following the pipeline in Section 5.3, we evaluate ACS with adaptive model selection, the naive method, CS-logistic, CS-RF, and CS-XGBRF. In this experiment, ACS adaptively selects the prediction model $\mathcal{G} \in \{\texttt{logistic}, \texttt{RF}, \texttt{XGBRF}\}$ every $L = 20$ steps. We plot the

[2] Generations are based on top-p sampling for each input X_i following the default configuration.

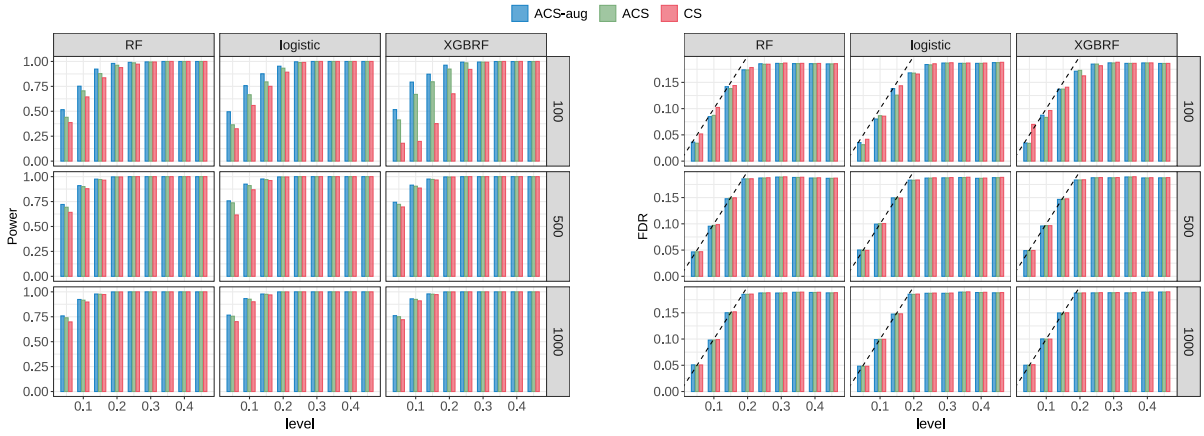


Figure 9: Realized power (left) and FDR (right) of ACS with new labels (ACS-aug), ACS without new labels (ACS), and CS from experiments on the CoQA dataset with LLaMA-2-13B-chat as the base LLM. Each column corresponds to a model class and each row corresponds to the size N of labeled samples. The target FDR level is $\alpha = 0.1$ and the results are averaged over 200 independent simulations.

realized power and FDR in Figure 10 from experiments on the CoQA dataset with LLaMA-2-13B-chat as the base LLM (results for TriviaQA are deferred to Appendix D.1). In both cases, we see that ACS with adaptive model selection achieves the highest power compared to the baselines while controlling FDR at the target level. Again, the advantage is more pronounced when the sample size N is small, or when the target FDR level is stringent.

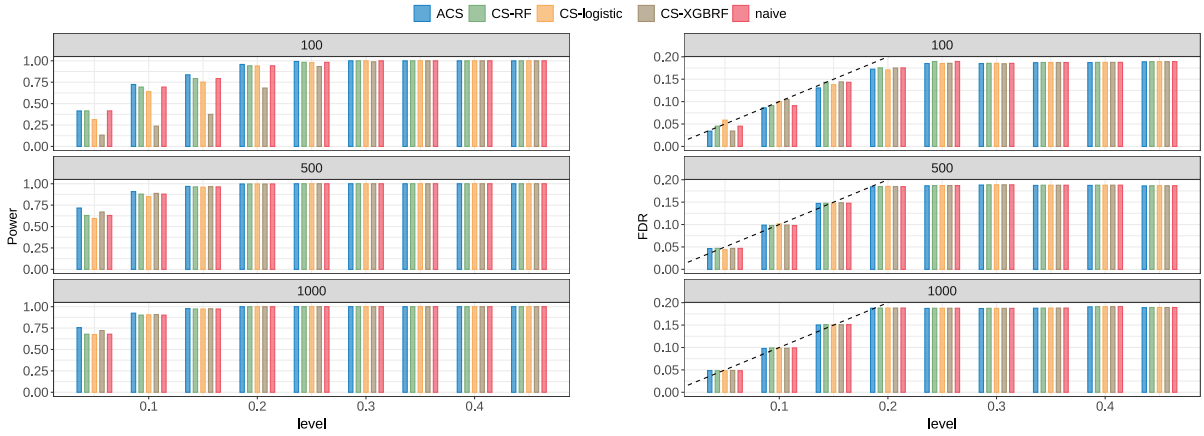


Figure 10: Realized power (left) and FDR (right) of ACS with adaptive model selection, the naive method, CS-SVR, CS-RF, and CS-GB from experiments on the CoQA dataset with LLaMA-2-13B-chat as the base LLM. Each subplot corresponds to the size N of labeled samples. The target FDR level is $\alpha = 0.1$ and the results are averaged over 200 independent simulations.

6.2 Experiments for chest X-ray report generation

We now turn to the task of chest X-ray report generation, where we aim to select a subset of machine-generated radiology reports that are aligned with expert evaluations. We evaluate the performance of ACS on the chest X-ray (CXR) dataset, which is a subset of the MIMIC-CXR dataset (Johnson et al., 2019) consisting of chest radiographs and radiology reports. Given an input image X_i, a fine-tuned vision language model (VLM) with a pre-trained VisionTransformer as image encoder and the GPT2 as the text generator is used to generate radiology reports, $f(X_i)$. To measure the alignment between VLM-generated and expert-written reports, we use CheXbert (Smit et al., 2004) to map both kinds of reports to 14-dimensional categorical vectors and the alignment score $Y_j = 1$ if and only if there are at least 12 matched labels. Base classifers and experimental setups are the same with Section 6.1.

ACS and ACS-aug with individual base models. In Figure 11, we compare the performance of CS, ACS, and ACS-aug across different base classifiers: `RF`, `logistic`, and `XGBRF`. In this limited-data setting, ACS consistently achieves higher power than CS, and ACS-aug further boosts power by increasing the effective sample size. The performance gain is particularly obvious when the sample size N is small and the classifier is more data-intensive, such as `XGBRF`.

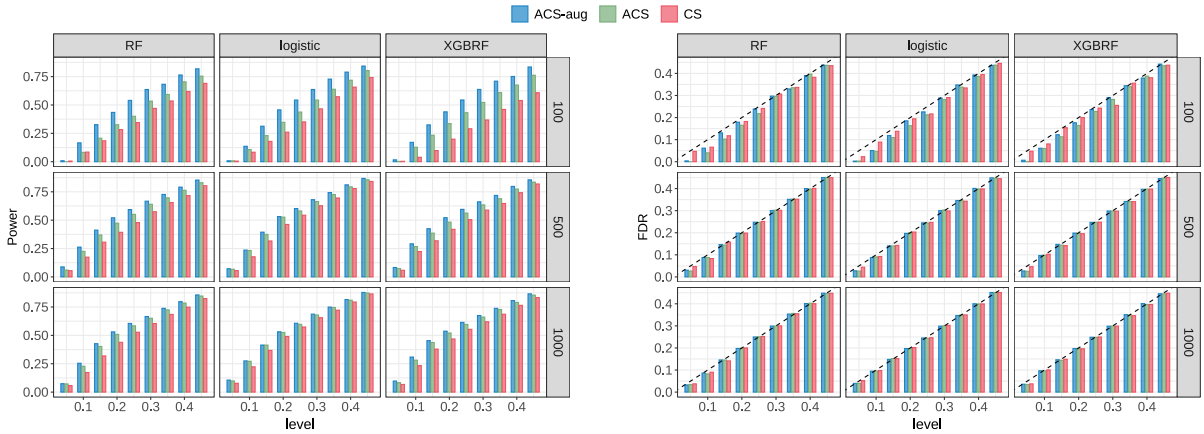


Figure 11: Realized power (left) and FDR (right) of ACS with new labels (ACS-aug), ACS without new labels (ACS), and CS from experiments on the MIMIC-CXR dataset. Each column corresponds to a model class and each row corresponds to the size N of labeled samples. The target FDR level is $\alpha = 0.1$ and the results are averaged over 200 independent simulations.

ACS with adaptive model selection. We further enhance the performance of ACS via adaptive model selection following Section 5.3 and compare its performance with CS using fixed base classifiers in Figure 12. In this task, the performance of the base models are largely similar, so the naive approach leads to little improvement. However, ACS with adaptive model selection still achieves visible power improvement while tightly controlling the FDR.

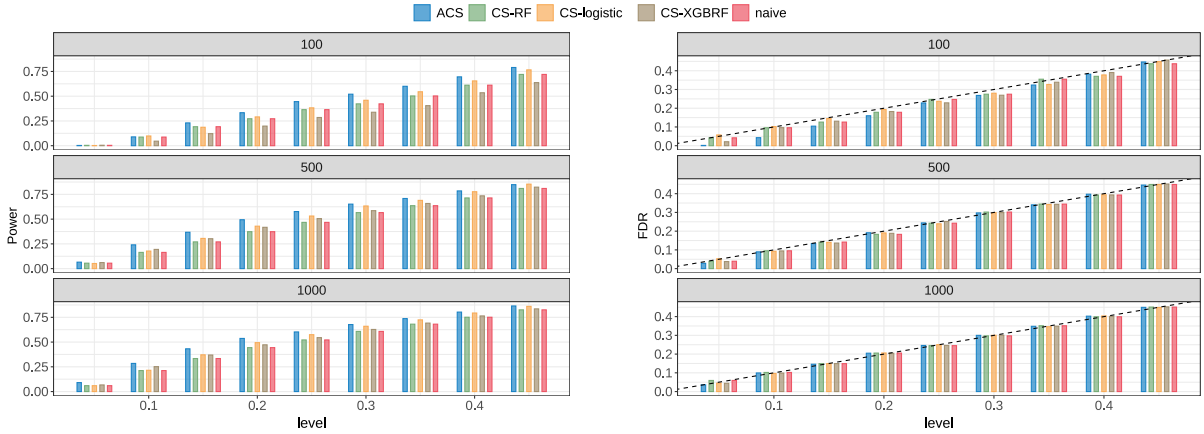


Figure 12: Realized power (left) and FDR (right) of ACS with adaptive model selection, the naive method, CS-SVR, CS-RF, and CS-GB: MIMIC-CXR dataset. Each subplot corresponds to the size N of labeled samples. The target FDR level is $\alpha = 0.1$ and the results are averaged over 200 independent simulations.

7 Real data application: Drug discovery

In this section, we use ACS to make diverse selections on a drug discovery dataset, where we will follow the notation in Section 4.2.1. Our experiments are performed on a catalytic receptor interaction dataset

from Alexander et al. (2023), consisting of ligand-receptor pairs (X) along with the binding affinity (Y) of each pair; large binding affinities indicate molecular potency, and the goal is to select a subset of ligand-receptor pairs with high binding affinity. Our goal will be to return a selection that is diverse as measured by the chemical similarity between ligands. More specifically, writing the pair as $X = (X_{\text{ligand}}, X_{\text{receptor}})$, we aim to return a selection set that contains a diverse set of X_{ligand}'s. To this end, we measure similarity between the X_{ligand}'s via the Tanimoto similarity (Tanimoto, 1958; Bajusz et al., 2015) between their fingerprints. Following Jin and Candès (2023b), we consider the property sets $\mathcal{C}_i = (-\infty, c_i]$ where c_i is the q-quantile of binding affinities in the training set with the same target receptor as that of the i^{th} example.

The machine learning algorithm we use to make quality predictions is a small neural network architecture. This model is a regressor and as such, we obtain the property set non-inclusion predicted probabilities $\widehat{\delta}_j \in [0, 1]$ by taking softmax. More specifically, if the remaining candidates are $i = 1, \ldots, \tilde{n}$, then we take

$$\widehat{\delta}_i = \frac{\exp(\widehat{g}(X_i))}{\sum_{j=1}^{\tilde{n}} \exp(\widehat{g}(X_j))}, \quad i = 1, \ldots, \tilde{n},$$

where $\widehat{g}$ is the fitted neural network regressor at the current screening step.

To proceed, we use a variant of the diversity-aware screening introduced in Section 4.2.1 with the FDR constraint turned off:

$$\begin{aligned} \min_{\xi} \ & \frac{\sum_{i,j=1}^{\tilde{n}} \xi_i \xi_j \widehat{\delta}_i \widehat{\delta}_j \cdot \theta(X_i, X_j)}{\sum_{i,j=1}^{\tilde{n}} \xi_i \xi_j \widehat{\delta}_i \widehat{\delta}_j} \\ \text{s.t. } & 0 \le \xi_i \le 1, \quad i = 1, \ldots, \tilde{n} \end{aligned} \tag{5}$$

Using a similar proof to that of Proposition 1, it can be shown that the program (5) can be reduced to

$$\begin{aligned} \min_{\xi} \ & \xi^\top \Theta \xi \\ \text{s.t. } & \xi_i \ge 0, \quad i = 1, \ldots, \tilde{n} \\ & \xi^\top \widehat{\delta} = 1 \end{aligned}$$

which is a quadratic program and can be efficiently solved. Finally, just as in Section 5.4, we actually determine the order of the remaining units by $\lambda \xi_{\text{work}} + (1 - \lambda)\widehat{\delta}$ and take $\lambda = 0.8$ in our experiments.

Our results are averaged over 250 random train/calibration/test splits of sizes 113, 113, and 225, respectively and the version of CS to which we compare uses the p-value described in Section 2.2 (as opposed to those involving uniform tie-breaking random variables).

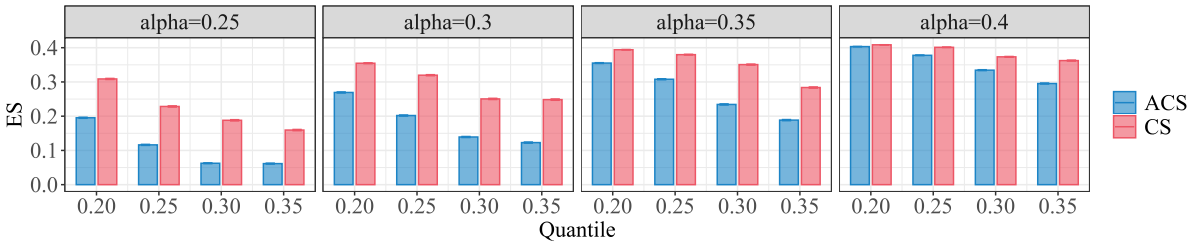


Figure 13: ES of ACS (blue) compared to CS (red) for various quantile values q and nominal FDR levels α on real drug discovery dataset. The results are averaged over 250 random train/calibration/test splits.

Figure 13 shows the ES of our method compared to CS for various values of $q \in \{0.2, 0.25, 0.3, 0.35\}$ as well as the nominal FDR level $\alpha \in \{0.25, 0.3, 0.35, 0.4\}$. The general takeaway is that ACS with diversity-aware ordering produces selection sets with lower expected similarity than CS. Interestingly, the gap between the effective similarities of ACS and CS shrinks as both the nominal level α increases and the quantile q decreases. This is most likely a reflection of the fact that the selection problem becomes easier for large α and small q, thereby allowing the FDP estimator to more easily fall below α at early timesteps. Indeed, this is reflected by the power plot given in Figure 14, which shows that the power of both methods in these settings is either equal to or very near one. We defer results showing the FDR of both methods to Appendix D.2.

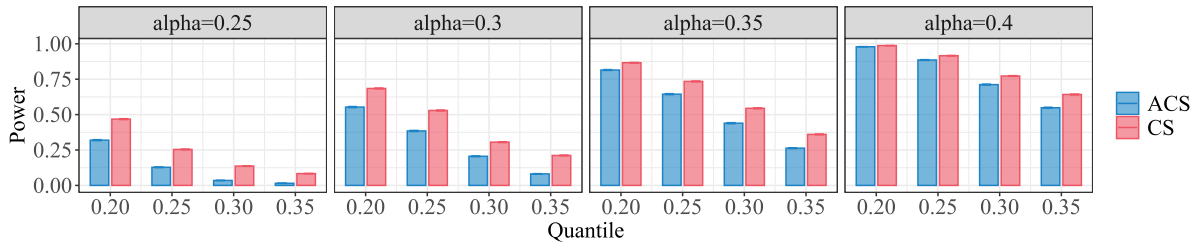


Figure 14: Power of ACS (blue) compared to CS (red) for various quantile values q and nominal FDR levels α on real drug discovery dataset. The other details are the same as in Figure 13.

8 Discussion

This work introduces ACS, a model-free selection algorithm offering both flexibility and rigorous control of FDR. The proposed framework allows for dynamic model update and selection, incorporating new information to maximize the selection power, and/or adapting to other utility functions determined by the practitioners. We demonstrate the performance of ACS in a variety of simulated settings and two real applications, showing that it outperforms existing methods in multiple dimensions. We conclude this paper by discussing some interesting directions for future research.

Extension to outlier detection. The idea behind the proposed ACS framework can be extended to the outlier detection problem, where the goal is to identify a set of outliers from a given dataset, relative to a set of inliers (Bates et al., 2023; Marandon et al., 2024). In outlier detection problems, it would be interesting to investigate the modelling approaches that are beneficial for the selection of outliers.

Other utility functions. This work mainly focuses on maximizing the power and/or diversity of the selected set. Given the flexibity of our framework, it is possible to aim for other utilities that appear in different applications (e.g., achieving conditional guarantees, minimizing user-specified risk functions).

Fully online selection. One limitation of the current ACS framework is that it does not accommodate the scenario where the test data arrives sequentially. An interesting direction for future research is to study an online version of ACS that can adaptively update the model and incorporate new information while maintaining appropriate type-I error controls.

Reproducibility

Code for reproducing the numerical results in this paper is available at https://github.com/zhimeir/acs_paper.

Acknowledgments

The authors would like to thank the Wharton Research Computing team for the computational resources provided and the great support from the staff members. Z. R. is supported by the National Science Foundation (NSF) under grant DMS-2413135 and Wharton Analytics. Y. N. acknowledges support by a Graduate Research Fellowship from the National Science Foundation.

References

Alexander, S. P. H., Fabbro, D., Kelly, E., Mathie, A. A., Peters, J. A., Veale, E. L., Armstrong, J. F., Faccenda, E., Harding, S. D., Davies, J. A., Beuve, A., Brouckaert, P., Bryant, C., Burnett, J. C., Farndale, R. W., Friebe, A., Garthwaite, J., Hobbs, A. J., Jarvis, G. E., Koesling, D., Kuhn, M., MacEwan, D., Monie, T. P., Potter, L. R., Russwurm, M., Schmidt, H. H. H. W., Stasch, J.-P., and Waldman, S. A. (2023). *British Journal of Pharmacology*, 180(S2):S241–S288.

Bai, T. and Jin, Y. (2024). Optimized conformal selection: Powerful selective inference after conformity score optimization. *arXiv preprint arXiv:2411.17983*.

Bai, T., Tang, P., Xu, Y., Svetnik, V., Khalili, A., Yu, X., and Yang, A. (2024). Conformal selection for efficient and accurate compound screening in drug discovery.

Bajusz, D., Rácz, A., and Héberger, K. (2015). Why is tanimoto index an appropriate choice for fingerprint-based similarity calculations? *Journal of cheminformatics*, 7:1–13.

Balakrishnan, B. D. A. R. S. and Wasserman, L. (2019). Interactive martingale tests for the global null. *arXiv preprint arXiv:1909.07339*.

Bashari, M., Epstein, A., Romano, Y., and Sesia, M. (2024). Derandomized novelty detection with fdr control via conformal e-values. *Advances in Neural Information Processing Systems*, 36.

Bashari, M., Sesia, M., and Romano, Y. (2025). Robust conformal outlier detection under contaminated reference data. *arXiv preprint arXiv:2502.04807*.

Bates, S., Candès, E., Lei, L., Romano, Y., and Sesia, M. (2023). Testing for outliers with conformal p-values. *The Annals of Statistics*, 51(1):149–178.

Benjamini, Y. and Hochberg, Y. (1995). Controlling the false discovery rate: a practical and powerful approach to multiple testing. *Journal of the Royal statistical society: series B (Methodological)*, 57(1):289–300.

Chao, P. and Fithian, W. (2021). Adapt-gmm: Powerful and robust covariate-assisted multiple testing. *arXiv preprint arXiv:2106.15812*.

Duan, B., Ramdas, A., and Wasserman, L. (2020). Familywise error rate control by interactive unmasking. In *International Conference on Machine Learning*, pages 2720–2729. PMLR.

Dwork, C., Feldman, V., Hardt, M., Pitassi, T., Reingold, O., and Roth, A. L. (2015). Preserving statistical validity in adaptive data analysis. In *Proceedings of the forty-seventh annual ACM symposium on Theory of computing*, pages 117–126.

Gui, Y., Jin, Y., and Ren, Z. (2024). Conformal alignment: Knowing when to trust foundation models with guarantees. *arXiv preprint arXiv:2405.10301*.

Huang, Z. (2007). *Drug discovery research: new frontiers in the post-genomic era*. John Wiley & Sons.

Huo, Y., Lu, L., Ren, H., and Zou, C. (2024). Real-time selection under general constraints via predictive inference. In *The Thirty-eighth Annual Conference on Neural Information Processing Systems*.

Jin, Y. and Candès, E. J. (2023a). Model-free selective inference under covariate shift via weighted conformal p-values. *arXiv preprint arXiv:2307.09291*.

Jin, Y. and Candès, E. J. (2023b). Selection by prediction with conformal p-values. *Journal of Machine Learning Research*, 24(244):1–41.

Johnson, A. E., Pollard, T. J., Berkowitz, S. J., Greenbaum, N. R., Lungren, M. P., Deng, C.-y., Mark, R. G., and Horng, S. (2019). Mimic-cxr, a de-identified publicly available database of chest radiographs with free-text reports. *Scientific data*, 6(1):317.

Joshi, M., Choi, E., Weld, D. S., and Zettlemoyer, L. (2017). Triviaqa: A large scale distantly supervised challenge dataset for reading comprehension. *arXiv preprint arXiv:1705.03551*.

Kadavath, S., Conerly, T., Askell, A., Henighan, T., Drain, D., Perez, E., Schiefer, N., Hatfield-Dodds, Z., DasSarma, N., Tran-Johnson, E., et al. (2022). Language models (mostly) know what they know. *arXiv preprint arXiv:2207.05221*.

Kuhn, L., Gal, Y., and Farquhar, S. (2023). Semantic uncertainty: Linguistic invariances for uncertainty estimation in natural language generation. *arXiv preprint arXiv:2302.09664*.

Lavecchia, A. and Di Giovanni, C. (2013). Virtual screening strategies in drug discovery: a critical

review. *Current medicinal chemistry*, 20(23):2839–2860.

Lee, J., Popov, I., and Ren, Z. (2025a). Full-conformal novelty detection: A powerful and non-random approach. *arXiv preprint arXiv:2501.02703*.

Lee, Y., Dobriban, E., and Tchetgen, E. T. (2025b). Finding distributions that differ, with false discovery rate control. *arXiv preprint arXiv:2505.13769*.

Lee, Y. and Ren, Z. (2025). Selection from hierarchical data with conformal e-values. *arXiv preprint arXiv:2501.02514*.

Lei, J., Rinaldo, A., and Wasserman, L. (2015). A conformal prediction approach to explore functional data. *Annals of Mathematics and Artificial Intelligence*, 74:29–43.

Lei, L. and Fithian, W. (2018). Adapt: an interactive procedure for multiple testing with side information. *Journal of the Royal Statistical Society Series B: Statistical Methodology*, 80(4):649–679.

Lei, L., Ramdas, A., and Fithian, W. (2021). A general interactive framework for false discovery rate control under structural constraints. *Biometrika*, 108(2):253–267.

Liang, Z., Sesia, M., and Sun, W. (2024). Integrative conformal p-values for out-of-distribution testing with labelled outliers. *Journal of the Royal Statistical Society Series B: Statistical Methodology*, 86(3):671–693.

Lin, C.-Y. (2004). Rouge: A package for automatic evaluation of summaries. In *Text summarization branches out*, pages 74–81.

Lin, Z., Trivedi, S., and Sun, J. (2023). Generating with confidence: Uncertainty quantification for black-box large language models. *arXiv preprint arXiv:2305.19187*.

Marandon, A., Lei, L., Mary, D., and Roquain, E. (2024). Adaptive novelty detection with false discovery rate guarantee. *The Annals of Statistics*, 52(1):157–183.

Mary, D. and Roquain, E. (2022). Semi-supervised multiple testing. *Electronic Journal of Statistics*, 16(2):4926–4981.

Nair, Y., Jin, Y., Yang, J., and Candes, E. (2025). Diversifying conformal selections. *arXiv preprint arXiv:2506.16229*.

Papadopoulos, H., Proedrou, K., Vovk, V., and Gammerman, A. (2002). Inductive confidence machines for regression. In *Machine learning: ECML 2002: 13th European conference on machine learning Helsinki, Finland, August 19–23, 2002 proceedings 13*, pages 345–356. Springer.

Pedregosa, F., Varoquaux, G., Gramfort, A., Michel, V., Thirion, B., Grisel, O., Blondel, M., Prettenhofer, P., Weiss, R., Dubourg, V., et al. (2011). Scikit-learn: Machine learning in python. *the Journal of machine Learning research*, 12:2825–2830.

Reddy, S., Chen, D., and Manning, C. D. (2019). Coqa: A conversational question answering challenge. *Transactions of the Association for Computational Linguistics*, 7:249–266.

Ren, Z. and Candès, E. (2023). Knockoffs with side information. *The Annals of Applied Statistics*, 17(2):1152–1174.

Roy, S., Bogomolov, M., Heller, R., Claridge, A. M., Beeson, T., and Small, D. S. (2025). Exploration, confirmation, and replication in the same observational study: A two team cross-screening approach to studying the effect of unwanted pregnancy on mothers' later life outcomes. *arXiv preprint arXiv:2505.14480*.

Sajjadiani, S., Sojourner, A. J., Kammeyer-Mueller, J. D., and Mykerezi, E. (2019). Using machine learning to translate applicant work history into predictors of performance and turnover. *Journal of Applied Psychology*, 104(10):1207.

Smit, A., Jain, S., Rajpurkar, P., Pareek, A., Ng, A., and Lungren, M. (2004). Chexbert: Combining automatic labelers and expert annotations for accurate radiology report labeling using bert. arxiv [cscl]. published online april 20, 2020.

Tanimoto, T. T. (1958). Elementary mathematical theory of classification and prediction.

Tian, X. and Taylor, J. (2018). Selective inference with a randomized response. *The Annals of Statistics*, 46(2):679–710.

Touvron, H., Martin, L., Stone, K., Albert, P., Almahairi, A., Babaei, Y., Bashlykov, N., Batra, S.,

Bhargava, P., Bhosale, S., et al. (2023). Llama 2: Open foundation and fine-tuned chat models. *arXiv preprint arXiv:2307.09288*.

Vovk, V., Gammerman, A., and Shafer, G. (2005). *Algorithmic learning in a random world*, volume 29. Springer.

Weinstein, A., Barber, R., and Candes, E. (2017). A power and prediction analysis for knockoffs with lasso statistics. *arXiv preprint arXiv:1712.06465*.

Wu, X., Huo, Y., Ren, H., and Zou, C. (2024). Optimal subsampling via predictive inference. *Journal of the American Statistical Association*, 119(548):2844–2856.

Xie, R., Barber, R., and Candes, E. (2024). Boosted conformal prediction intervals. *Advances in Neural Information Processing Systems*, 37:71868–71899.

Xiong, M., Hu, Z., Lu, X., Li, Y., Fu, J., He, J., and Hooi, B. (2023). Can llms express their uncertainty? an empirical evaluation of confidence elicitation in llms. *arXiv preprint arXiv:2306.13063*.

Xu, Z. and Ramdas, A. (2024). Online multiple testing with e-values. In *International Conference on Artificial Intelligence and Statistics*, pages 3997–4005. PMLR.

Yang, C.-Y., Lei, L., Ho, N., and Fithian, W. (2021). Bonus: Multiple multivariate testing with a data-adaptivetest statistic. *arXiv preprint arXiv:2106.15743*.

Yang, Y., Ma, Z., Nie, F., Chang, X., and Hauptmann, A. G. (2015). Multi-class active learning by uncertainty sampling with diversity maximization. *International Journal of Computer Vision*, 113:113–127.

Zhang, S., Roller, S., Goyal, N., Artetxe, M., Chen, M., Chen, S., Dewan, C., Diab, M., Li, X., Lin, X. V., et al. (2023). Opt: Open pre-trained transformer language models, 2022. *URL https://arxiv.org/abs/2205.01068*, 3:19–0.

Zhao, Z., Wallace, E., Feng, S., Klein, D., and Singh, S. (2021). Calibrate before use: Improving few-shot performance of language models. In *International conference on machine learning*, pages 12697–12706. PMLR.

Zhong, P., Gong, Z., Li, S., and Schönlieb, C.-B. (2017). Learning to diversify deep belief networks for hyperspectral image classification. *IEEE Transactions on Geoscience and Remote Sensing*, 55(6):3516–3530.

A Proofs of the main results

A.1 Proof of Theorem 1

For notational convenience, we further define $P_\ell^- = P_\ell \cap \mathcal{H}_0$ and $P_\ell^+ = P_\ell \backslash P_\ell^-$. By the definition of FDR and the choice of the stopping time T, we have

$$\begin{aligned}\mathrm{FDR} = \mathbb{E}\left[\frac{|P_T^-|}{|P_T| \vee 1}\right] &= \mathbb{E}\left[\frac{m}{n-k+1}\frac{1+|N_T^-|}{|P_T| \vee 1} \cdot \frac{n-k+1}{m}\frac{|P_T^-|}{1+|N_T^-|}\right] \\ &= \mathbb{E}\left[\widehat{\mathrm{FDP}}(T) \cdot \frac{n-k+1}{m}\frac{|P_T^-|}{1+|N_T^-|}\right] \\ &\le \frac{\alpha(n-k+1)}{m}\mathbb{E}\left[\frac{|P_T^-|}{1+|N_T^-|}\right].\end{aligned}$$

Next, we define

$$M_\ell := \frac{|P_\ell^-|}{1+|N_\ell^-|} \text{ and } \mathcal{G}_\ell = \sigma\Big\{O_\ell, N_k^+, |N_\ell^-|, |P_\ell^+|, |P_\ell^-|, \{(Z_i, A_i)\}_{i \in O_\ell \cup N_k^+}, \{X_i\}_{i \in U_\ell}\Big\}$$

It can be checked $\{\mathcal{G}_\ell\}_{\ell \ge k}$ is a filtration, and that M_ℓ is $\mathcal{G}_\ell$-measurable. It can also be observed that $\mathcal{F}_\ell \subseteq \mathcal{G}_\ell$, $\forall \ell \ge k$. We shall then show that $\{M_\ell\}_{\ell \ge k}$ is a super-martingale sequence with respect to $\{\mathcal{G}_\ell\}_{\ell \ge k}$, and then apply the optional stopping theorem to conclude the proof.

To see that $\{M_\ell\}_{\ell \ge k}$ is a super-martingale sequence, we fix $\ell \ge k$ and check the conditional expectation:

$$\begin{aligned}\mathbb{E}[M_{\ell+1} \,|\, \mathcal{G}_\ell] &= \mathbb{E}\left[\frac{|P_{\ell+1}^-|}{1+|N_{\ell+1}^-|} \,\middle|\, \mathcal{G}_\ell\right] \\ &\overset{\text{(a)}}{=} \mathbb{E}\left[\mathbb{1}\big\{Y_{\pi(\ell+1)} \notin \mathcal{C}_{\pi(\ell+1)}\big\}\frac{|P_\ell^-|}{1+|N_\ell^-|} \,\middle|\, \mathcal{G}_\ell\right] + \mathbb{E}\left[\mathbb{1}\big\{Y_{\pi(\ell+1)} \in \mathcal{C}_{\pi(\ell+1)}, A_{\pi(\ell+1)} = 0\big\}\frac{|P_\ell^-|}{|N_\ell^-|} \,\middle|\, \mathcal{G}_\ell\right] \\ &\quad + \mathbb{E}\left[\mathbb{1}\big\{Y_{\pi(\ell+1)} \in \mathcal{C}_{\pi(\ell+1)}, A_{\pi(\ell+1)} = 1\big\}\frac{|P_\ell^-|-1}{1+|N_\ell^-|} \,\middle|\, \mathcal{G}_\ell\right] \\ &\overset{\text{(b)}}{=} \frac{|P_\ell^-|}{1+|N_\ell^-|} \cdot \mathbb{P}\big(Y_{\pi(\ell+1)} \notin \mathcal{C}_{\pi(\ell+1)} \,|\, \mathcal{G}_\ell\big) + \frac{|P_\ell^-|}{|N_\ell^-|} \cdot \mathbb{P}\big(Y_{\pi(\ell+1)} \in \mathcal{C}_{\pi(\ell+1)}, A_{\pi(\ell+1)} = 0 \,|\, \mathcal{G}_\ell\big) \\ &\quad + \frac{|P_\ell^-|-1}{1+|N_\ell^-|} \cdot \mathbb{P}\big(Y_{\pi(\ell+1)} \in \mathcal{C}_{\pi(\ell+1)}, A_{\pi(\ell+1)} = 1 \,|\, \mathcal{G}_\ell\big). \qquad (6)\end{aligned}$$

Above, step (a) is by the definition of P_ℓ^- and N_ℓ^-; step (b) is since $|P_\ell^-|$ and $|N_\ell^-|$ are $\mathcal{G}_\ell$-measurable.

To proceed, we need the following lemma, which states that conditional on $\mathcal{G}_\ell$, any of the unscreened *null* samples is equally likely to be selected as $\pi(\ell+1)$. Its proof is deferred to Appendix B.1.

Lemma 1. *For any $\ell \ge k$,*

$$\begin{aligned}\mathbb{P}(A_{\pi(\ell+1)} = 0 \,|\, \mathcal{G}_\ell, Y_{\pi(\ell+1)} \in \mathcal{C}_{\pi(\ell+1)}) &= \frac{|N_\ell^-|}{|P_\ell^-| + |N_\ell^-|}, \\ \mathbb{P}(A_{\pi(\ell+1)} = 1 \,|\, \mathcal{G}_\ell, Y_{\pi(\ell+1)} \in \mathcal{C}_{\pi(\ell+1)}) &= \frac{|P_\ell^-|}{|P_\ell^-| + |N_\ell^-|}.\end{aligned}$$

Applying Lemma 1 to (6), we have

$$\begin{aligned}(6) = \frac{|P_\ell^-|}{1+|N_\ell^-|} \cdot \mathbb{P}\big(Y_{\pi(\ell+1)} \notin \mathcal{C}_{\pi(\ell+1)} \,|\, \mathcal{G}_\ell\big) &+ \frac{|P_\ell^-|}{|N_\ell^-|}\frac{|N_\ell^-|}{|N_\ell^-| + |P_\ell^-|} \cdot \mathbb{P}(Y_{\pi(\ell+1)} \in \mathcal{C}_{\pi(\ell+1)} \,|\, \mathcal{G}_\ell) \\ &+ \frac{|P_\ell^-|-1}{1+|N_\ell^-|}\frac{|P_\ell^-|}{|N_\ell^-| + |P_\ell^-|} \cdot \mathbb{P}(Y_{\pi(\ell+1)} \in \mathcal{C}_{\pi(\ell+1)} \,|\, \mathcal{G}_\ell)\end{aligned}$$

$$= \frac{|P_\ell^-|}{1+|N_\ell^-|} \cdot \mathbb{P}\big(Y_{\pi(\ell+1)} \notin \mathcal{C}_{\pi(\ell+1)} \,|\, \mathcal{G}_\ell\big) + \left(\frac{|P_\ell^-|}{|N_\ell^-|+|P_\ell^-|} + \frac{|P_\ell^-|(|P_\ell^-|-1)}{(1+|N_\ell^-|)(|N_\ell^-|+|P_\ell^-|)}\right) \cdot \mathbb{P}(Y_{\pi(\ell+1)} \in \mathcal{C}_{\pi(\ell+1)} \,|\, \mathcal{G}_\ell)$$
$$= \frac{|P_\ell^-|}{1+|N_\ell^-|} = M_\ell.$$

We have now established that $\{M_\ell\}_{\ell \geq k}$ is a super-martingale sequence with respect to the filtration $\{\mathcal{G}_\ell\}_{\ell \geq k}$. Since T is a stopping time with respect to the same filtration, we now apply the optional stopping theorem to conclude that $\mathbb{E}[M_T] \leq \mathbb{E}[M_k]$. We finish the proof by bounding $\mathbb{E}[M_k]$.

For notational convenience, define $n' := n - k$. Let $T_k^- := |P_k^-| + |N_k^-|$ denote the total number of null samples among the data not set aside in the initial training phase. We will condition on T_k^- and show that

$$\mathbb{E}[M_k \mid T_k^-] \leq \frac{m}{1+n'}, \tag{7}$$

from which the result immediately follows. To show (7), observe that the exchangeability between the labeled and test data implies that $|P_k^-| \,|\, T_k^- \sim \text{Hypergeom}(m+n', T_k^-, m)$.[3] Consequently, inequality (7) is a direct result of Lemma 2 below, whose proof can be found in Appendix B.2.

Lemma 2. *Let $X \sim$ Hypergeom$(m+n', \kappa, m)$ for any non-negative integer $\kappa \leq m+n'$. Then*

$$\mathbb{E}\left[\frac{X}{1+\kappa-X}\right] \leq \frac{m}{1+n'}$$

A.2 Proof of Proposition 1

Throughout the proof, we use $\mathbf{1}$ to denote the vector of ones of length $\tilde{n}$ without explicit dependence on $\tilde{n}$. Letting $\gamma_i = \xi_i / \xi^\top \widehat{\delta}$, we rewrite the optimization problem in (3) as

$$\begin{aligned} \min_\gamma \ & \gamma^\top \Theta \gamma, \\ \text{s.t.} \ & \gamma^\top \mathbf{1} = \frac{1}{1-\alpha}, \\ & \gamma^\top \widehat{\delta} = 1. \end{aligned}$$

The condition $\xi^\top \widehat{\delta} > 0$ vanishes since γ is agnostic to the sign of $\xi^\top \widehat{\delta}$. The Lagrangian of the above optimization problem is

$$\mathcal{L}(\gamma, \lambda, \mu) = \gamma^\top \Theta \gamma + \lambda\Big(\gamma^\top \mathbf{1} - \frac{1}{1-\alpha}\Big) + \mu(\gamma^\top \widehat{\delta} - 1),$$

where λ and μ are Lagrange multipliers. Letting $(\gamma^*, \lambda^*, \mu^*)$ be the optimal solution, the KKT condition yields that

$$\frac{\partial}{\partial \gamma}\mathcal{L}(\gamma^*, \lambda^*, \mu^*) = 2\Theta\gamma^* + \lambda^* \mathbf{1} + \mu^* \widehat{\delta} = 0 \Rightarrow \gamma^* = -\frac{1}{2}\Theta^{-1}(\lambda^* \mathbf{1} + \mu^* \widehat{\delta}).$$

The other two KKT conditions are

$$\begin{aligned} (\gamma^*)^\top \widehat{\delta} &= -\frac{1}{2}(\lambda^* a + \mu^* b) = 1, \\ (\gamma^*)^\top \mathbf{1} &= -\frac{1}{2}(\lambda^* c + \mu^* a) = \frac{1}{1-\alpha}. \end{aligned}$$

The above yields

$$\mu^* = \frac{2}{bc-a^2}\Big(\frac{a}{1-\alpha} - c\Big), \text{ and } \lambda^* = \frac{2}{bc-a^2}\Big(a - \frac{b}{1-\alpha}\Big).$$

Putting things together, we have

$$\gamma^* = \frac{1}{bc-a^2}\left[\Big(\frac{b}{1-\alpha} - a\Big)\Theta^{-1}\mathbf{1} + \Big(c - \frac{a}{1-\alpha}\Big)\Theta^{-1}\widehat{\delta}\right].$$

Recalling $\xi^* = \gamma^* \cdot (\xi^*)^\top \widehat{\delta}$, we have the desired result.

[3] As a reminder, the first parameter is the total population size, the second is the number of units labeled "success" (in our case, the number of units which are null samples), and the third is the number of draws.

B Proof of Additional Lemmas

B.1 Proof of Lemma 1

To show the claim, we are to prove a stronger statement: for any $\ell \geq k$, and any $i \in P_\ell^- \cup N_\ell^-$,

$$\mathbb{P}\big(\pi(\ell+1) = i \,|\, \mathcal{G}_\ell, Y_{\pi(\ell+1)} \in \mathcal{C}_{\pi(\ell+1)}\big) = \frac{1}{|P_\ell^-| + |N_\ell^-|}. \tag{8}$$

Recall that by construction, $\pi(\ell+1)$ is a function of the information in $\mathcal{G}_\ell$. Slightly abusing the notation, we write $\pi(\ell+1) := h_{\ell+1}(\mathcal{G}_\ell)$ for some measurable function $h_{\ell+1}$; we also define

$$\bar{\mathcal{G}}_\ell = \big(\bar{O}_\ell, \bar{N}_k^+, |\bar{N}_\ell^-|, |\bar{P}_\ell^+|, |\bar{P}_\ell^-|, \{(\bar{Z}_i, \bar{A}_i)\}_{i \in \bar{O}_\ell \cup \bar{N}_k^+}, \{\bar{X}_i\}_{i \in U_\ell}\big)$$

and $\bar{P}_\ell^+$ denote the realization of $\mathcal{G}_\ell$ and P_ℓ^+, respectively. Then

$$\begin{aligned}
&\mathbb{P}\big(\pi(\ell+1) = i \,|\, \mathcal{G}_\ell = \bar{\mathcal{G}}_\ell, P_\ell^+ = \bar{P}_\ell^+, Y_{\pi(\ell+1)} \in \mathcal{C}_{\pi(\ell+1)}\big) \\
&= \frac{\mathbb{P}\big(h_{\ell+1}(\bar{\mathcal{G}}_\ell) = i, \mathcal{G}_\ell = \bar{\mathcal{G}}_\ell, P_\ell^+ = \bar{P}_\ell^+, Y_{\pi(\ell+1)} \in \mathcal{C}_{\pi(\ell+1)}\big)}{\mathbb{P}\big(\mathcal{G}_\ell = \bar{\mathcal{G}}_\ell, P_\ell^+ = \bar{P}_\ell, Y_{\pi(\ell+1)} \in \mathcal{C}_{\pi(\ell+1)}\big)}.
\end{aligned}$$

For any $j \in \bar{P}_\ell^- \cup \bar{N}_\ell^-$, note that both $\mathcal{G}_\ell$ and P_ℓ^+ are invariant to the swapping of Z_i and Z_j. Also by exchangeability, swapping Z_i and Z_j does not change the joint distribution of the data points, and therefore

$$\begin{aligned}
&\mathbb{P}\big(h_{\ell+1}(\bar{\mathcal{G}}_\ell) = i, \mathcal{G}_\ell = \bar{\mathcal{G}}_\ell, P_\ell^+ = \bar{P}_\ell^+, Y_i \in \mathcal{C}_i\big) \\
&= \mathbb{P}\big(h_{\ell+1}(\bar{\mathcal{G}}_\ell) = j, \mathcal{G}_\ell = \bar{\mathcal{G}}_\ell, P_\ell^+ = \bar{P}_\ell^+, Y_j \in \mathcal{C}_j\big) \\
&= \frac{1}{|\bar{P}_\ell^-| + |\bar{N}_\ell^-|} \sum_{j \in \bar{P}_\ell^- \cup \bar{N}_\ell^-} \mathbb{P}\big(\pi(\ell+1) = j, \mathcal{G}_\ell = \bar{\mathcal{G}}_\ell, P_\ell^+ = \bar{P}_\ell^+, Y_{\pi(\ell+1)} \in \mathcal{C}_{\pi(\ell+1)}\big) \\
&= \frac{1}{|\bar{P}_\ell^-| + |\bar{N}_\ell^-|} \mathbb{P}\big(\mathcal{G}_\ell = \bar{\mathcal{G}}_\ell, P_\ell^+ = \bar{P}_\ell^+, Y_{\pi(\ell+1)} \in \mathcal{C}_{\pi(\ell+1)}\big),
\end{aligned}$$

which implies (8). Using (8), we finally arrive at

$$\begin{aligned}
&\mathbb{P}\big(A_{\pi(\ell+1)} = 1 \,|\, \mathcal{G}_\ell, Y_{\pi(\ell+1)} \in \mathcal{C}_{\pi(\ell+1)}\big) \\
&= \mathbb{E}\Big[\mathbb{P}\big(A_{\pi(\ell+1)} = 1 \,|\, \mathcal{G}_\ell, Y_{\pi(\ell+1)} \in \mathcal{C}_{\pi(\ell+1)}, P_\ell^+\big) \,\Big|\, \mathcal{G}_\ell, Y_{\pi(\ell+1)} \in \mathcal{C}_{\pi(\ell+1)}\Big] \\
&= \frac{|N_\ell^-|}{|N_\ell^-| + |P_\ell^-|},
\end{aligned}$$

completing the proof.

B.2 Proof of Lemma 2

We have that

$$\begin{aligned}
\mathbb{E}\left[\frac{X}{1+\kappa-X}\right] &= \sum_{x=\max(1,\kappa-n')}^{\min(m,\kappa)} \frac{x}{1+\kappa-x} \frac{\binom{\kappa}{x}\binom{m+n'-\kappa}{m-x}}{\binom{m+n'}{m}} \\
&= \sum_{x=\max(1,\kappa-n')}^{\min(m,\kappa)} \frac{\binom{\kappa}{x-1}\binom{m+n'-\kappa}{m-x}}{\binom{m+n'}{m}} \\
&= \sum_{x=\max(1,\kappa-n')}^{\min(m,\kappa)} \frac{\binom{\kappa}{x-1}\binom{m+n'-\kappa}{(m-1)-(x-1)}}{\binom{m+n'}{m-1} \cdot \frac{n'+1}{m}} \\
&= \frac{m}{n'+1} \sum_{x=\max(0,\kappa-(n'+1))}^{\min(m,\kappa)-1} \frac{\binom{\kappa}{x}\binom{m+n'-\kappa}{m-1-x}}{\binom{m+n'}{m-1}}
\end{aligned}$$

$$\leq \frac{m}{n'+1} \sum_{x=\max(0,\kappa-(n'+1))}^{\min(m-1,\kappa)} \frac{\binom{\kappa}{x}\binom{m+n'-\kappa}{m-1-x}}{\binom{m+n'}{m-1}}$$
$$= \frac{m}{n'+1},$$

where the final equality is due to the fact that the summation in the penultimate line is 1 as it is of the PMF of the Hypergeom$(m+n', \kappa, m-1)$ distribution across its support.

C Additional simulation results

This section contains additional simulation results. In addition to the data generating process described in Section 5 (referred to as Setting 1 hereafter), we investigate the performance of our proposed method under several other settings adapted from Jin and Candès (2023b). Supposing $Y_i \sim \mathcal{N}(\mu(X_i), \sigma(X_i)^2)$, we consider the following choices of $\mu(\cdot)$ and $\sigma(\cdot)$:

- Setting 2: $\mu(x) = 5(x_1x_2 + e^{x_4-1})$, $\sigma(x) = 1.5 \cdot \sigma$;
- Setting 3: $\mu(x) = 5(x_1x_2 + e^{x_4-1})$, $\sigma(x) = \sigma \cdot (5.5 - |\mu(x)|)/2$;
- Setting 4: $\mu(x) = 5(x_1x_2 + e^{x_4-1})$, $\sigma(x) = \sigma \cdot 0.25\mu(x)^2\mathbb{1}\{|\mu(x)| < 2\} + \sigma \cdot 0.5|\mu(x)|\mathbb{1}\{|\mu(x)| \geq 1\}$;
- Setting 5: $\mu(x) = 2(x_1x_2 + x_3^2 + e^{x_4-1} - 1)$, $\sigma(x) = 1.5 \cdot \sigma$.

Section C.1 contains the additional results of ACS with different individual base models under Settings 2-5. Section C.2 contains the results of ACS with model selection under Settings 2-5. Section C.3 provides the results of diversity-aware ACS with different choices of λ, while Section C.4 investigates the effect of the choice of k on the performance of ACS.

C.1 Additional results with individual base models

Figures 15–18 show the realized power and FDR of ACS and CS under Settings 2-5. The same story holds as in Setting 1: ACS uniformly outperforms CS in terms of realized power for diferrent individual base models or different samples sizes, while maintaining the FDR at the nominal level.

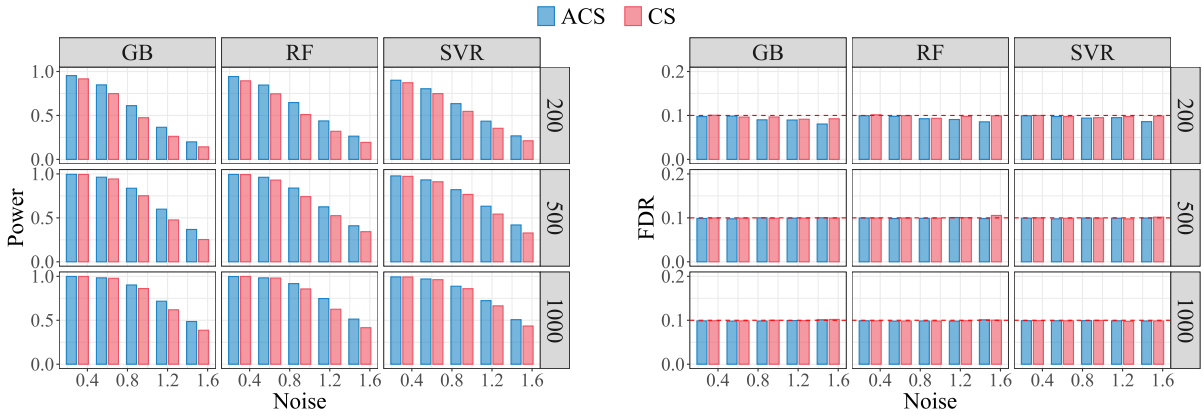


Figure 15: Realized power (left) and FDR (right) of ACS and CS under simulation Setting 2. The other details are the same as in Figure 4.

C.2 Model selection

Figures 19–22 plot the realized power and FDR of ACS with adaptive model selection, the naive method, CS-SCR, CS-RF, and CS-GB under Settings 2-5. In all settings considered, ACS dominates the best base models, as well as the naive method, showing its ability to automatically pick the best model. Once again, the FDR of ACS is well controlled at the nominal level.

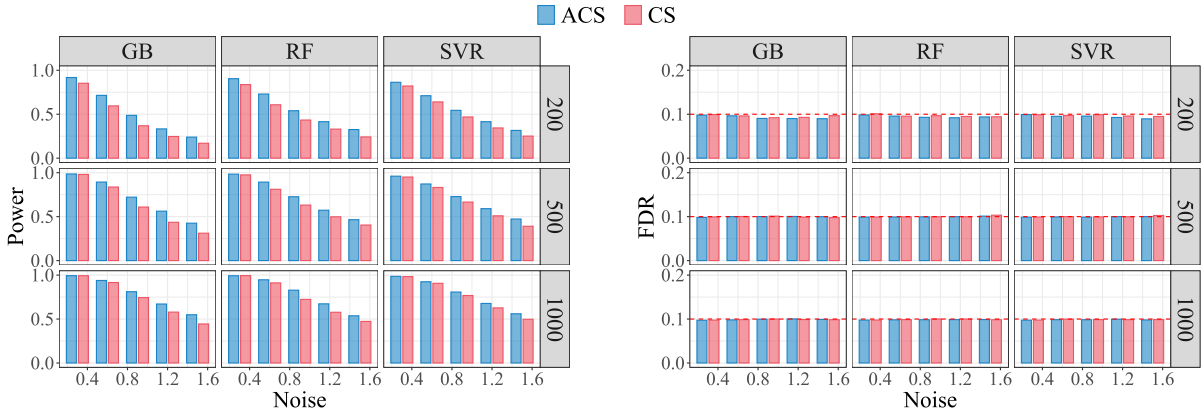


Figure 16: Realized power (left) and FDR (right) of ACS and CS under simulation Setting 3. The other details are the same as in Figure 4.

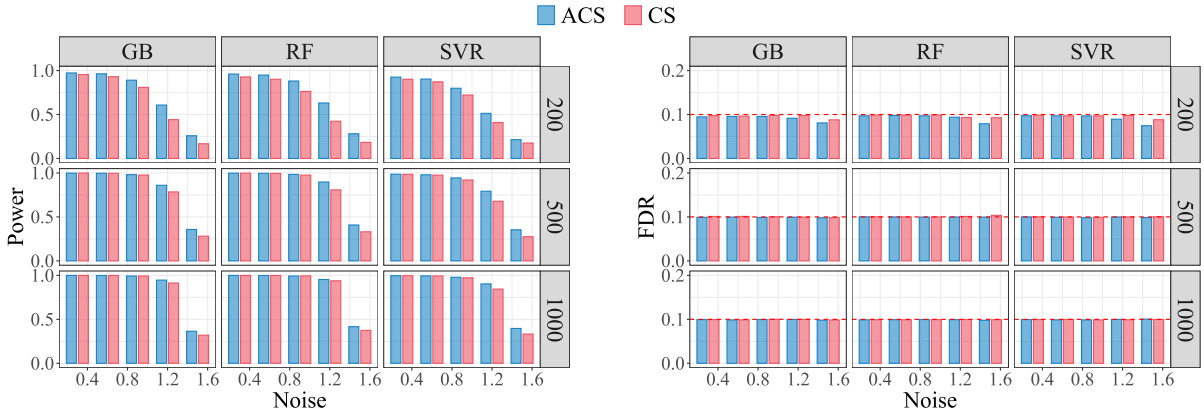


Figure 17: Realized power (left) and FDR (right) of ACS and CS under simulation Setting 4. The other details are the same as in Figure 4.

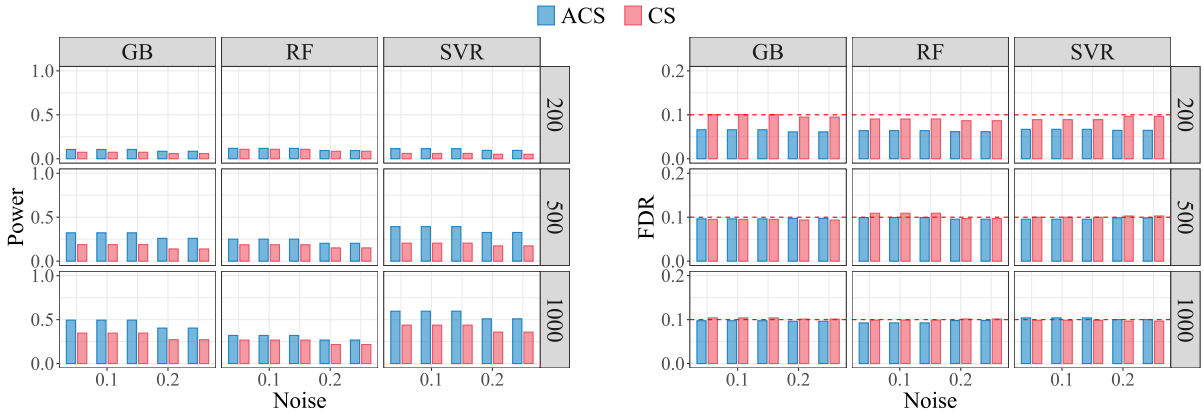


Figure 18: Realized power (left) and FDR (right) of ACS and CS under simulation Setting 5. The other details are the same as in Figure 4.

C.3 Diversity-aware selection

This section contains the results of diversity-aware ACS under Setting 1 with other choices of λ. Figures 23 and 25 plot the $\widehat{\text{ES}}$ as a function of $\widehat{\text{Power}}$; compared with the results in Figure 6, we can see that increasing λ leads to a decrease in the $\widehat{\text{ES}}$, reflecting a higher weight on the diversity term. Figures 24 and 26 show the realized power and FDR of diversity-aware ACS with $\lambda = 0.4$ and $\lambda = 0.5$, respectively. The power of ACS slightly decreases as λ increases—this is plausibly due to that the procedure refrains

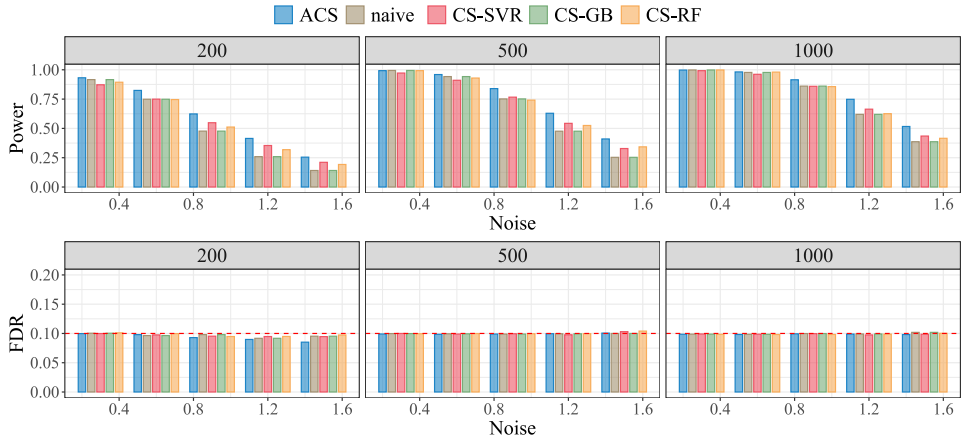


Figure 19: Realized power (left) and FDR (right) of ACS with adaptive model selection, the naive method, CS-SCR, CS-RF, and CS-GB as a function of the noise level σ under simulation Setting 2. The other details are the same as in Figure 5.

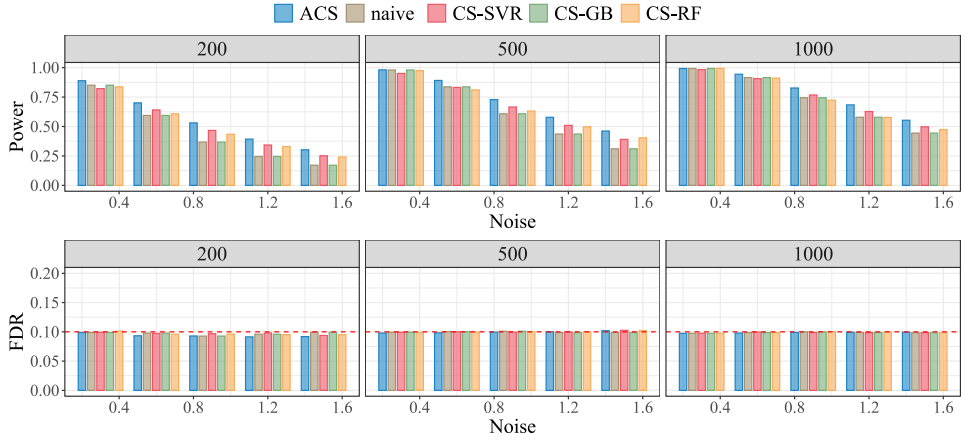


Figure 20: Realized power (left) and FDR (right) of ACS with adaptive model selection, the naive method, CS-SCR, CS-RF, and CS-GB as a function of the noise level σ under simulation Setting 3. The other details are the same as in Figure 5.

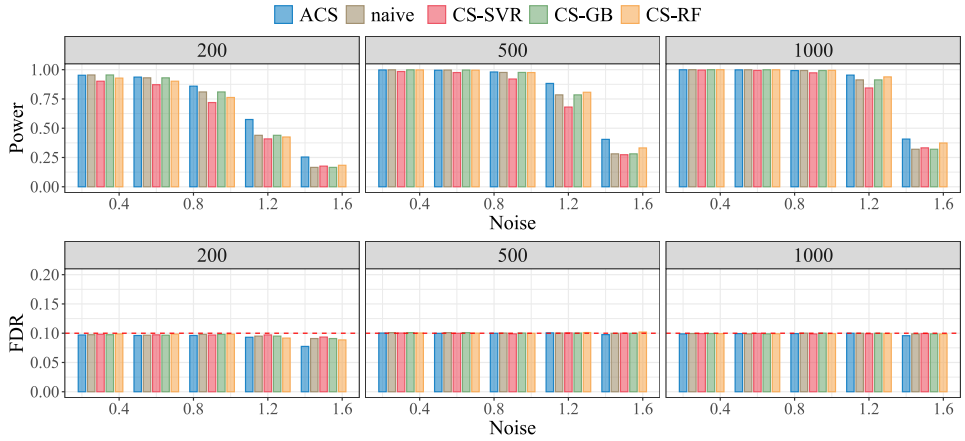


Figure 21: Realized power (left) and FDR (right) of ACS with adaptive model selection, the naive method, CS-SCR, CS-RF, and CS-GB as a function of the noise level σ under simulation Setting 4. The other details are the same as in Figure 5.

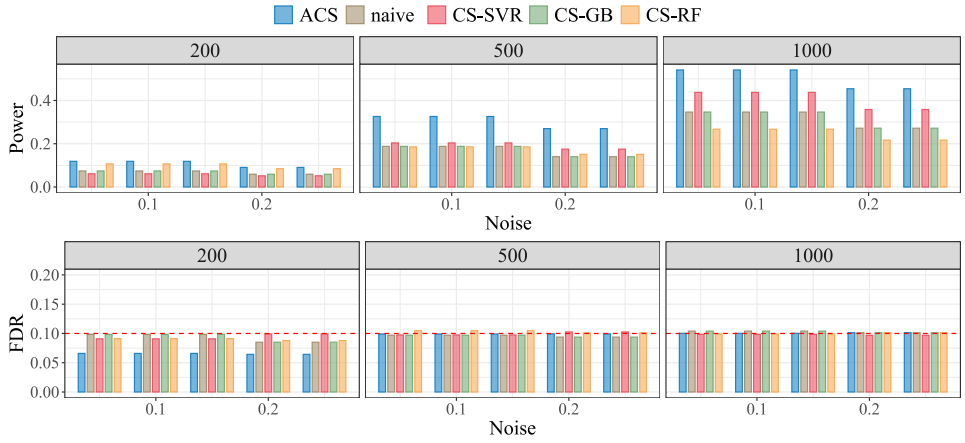


Figure 22: Realized power (left) and FDR (right) of ACS with adaptive model selection, the naive method, CS-SCR, CS-RF, and CS-GB as a function of the noise level σ under simulation Setting 5. The other details are the same as in Figure 5.

from making selections that are similar to the ones already made. The FDR remains controlled across different values of λ.

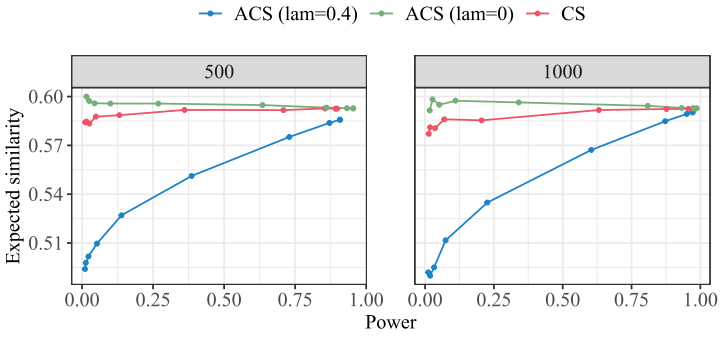


Figure 23: $\widehat{\text{ES}}$ as a function of $\widehat{\text{Power}}$ for diversity-aware ACS with $\lambda = 0.4$, ACS, and CS under Setting 1. The other details are the same as in Figure 6.

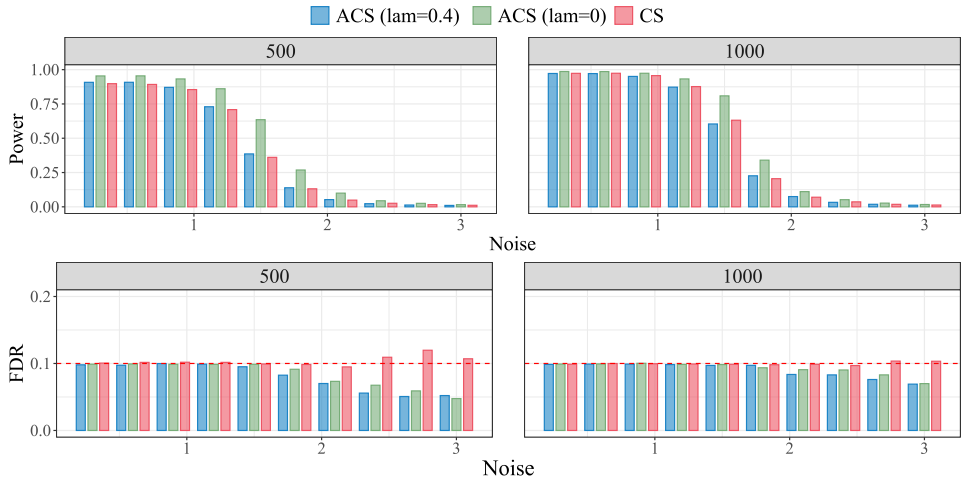


Figure 24: Realized power (left) and FDR (right) of diversity-aware ACS with $\lambda = 0.4$, ACS, and CS as a function of the noise level σ under simulation Setting 1. The other details are the same as in Figure 7.

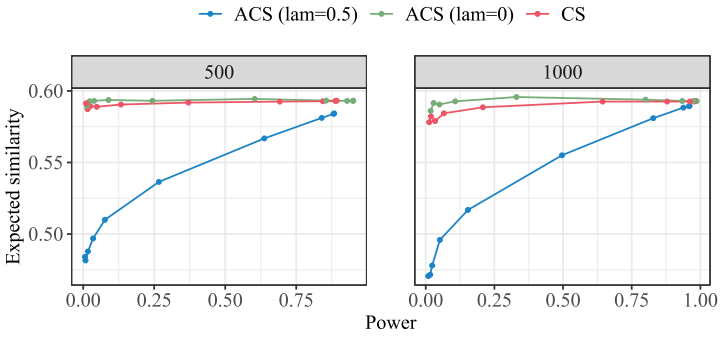


Figure 25: $\widehat{\text{ES}}$ as a function of $\widehat{\text{Power}}$ for diversity-aware ACS with $\lambda = 0.5$, ACS, and CS. The other details are the same as in Figure 6.

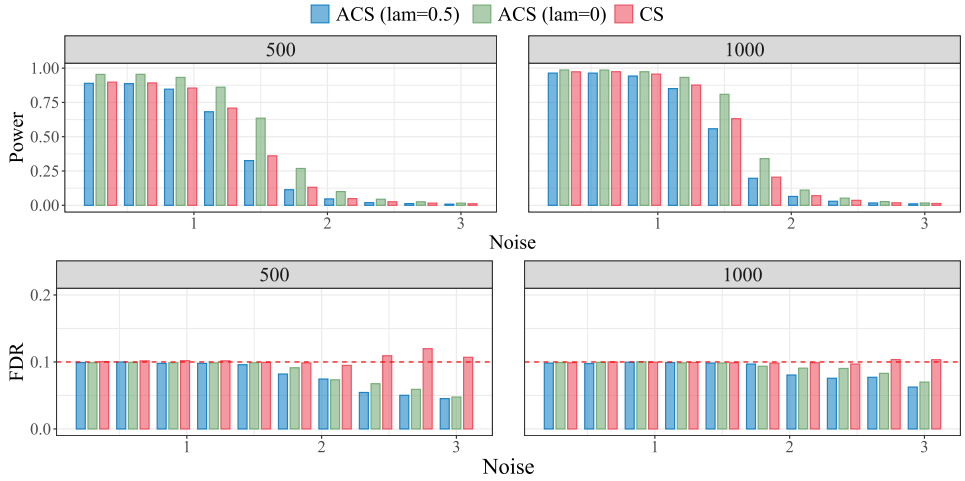


Figure 26: Realized power (left) and FDR (right) of diversity-aware ACS with $\lambda = 0.5$, ACS, and CS as a function of the noise level σ under simulation Setting 1. The other details are the same as in Figure 7.

C.4 The effect of k

Under Setting 1, we implement ACS with 200 labeled samples and k (the number of initial samples used to train the model) ranging in $\{60, 80, 100\}$. The results are visualized in Figure 27. The results do not differ significantly across different values of k.

D Additional real data results

D.1 Additional details and results for LLM deployment

In this section, we present more implementation details for Section 6 and additional results with a smaller model **OPT-13B**.

D.1.1 Feature engineering for prediction model training

Following Gui et al. (2024), to build the prediction model $\widehat{g}$, we use a separate tuning set $\mathcal{D}_{\text{tune}}$ for feature engineering. More specifically, we focus on quantities that are extracted from foundation model outputs. As the quality of the outputs can be affected by the difficulty of the task suggested by the prompt as well as LLM's capability in this specific task–which can be revealed in both the likelihood of the output and the confidence of the model itself, we consider the following quantities as the available covariates $\tilde{X}_j$:

- Self-evaluation likelihoods (Kadavath et al., 2022; Lin et al., 2023). The self-evaluation score

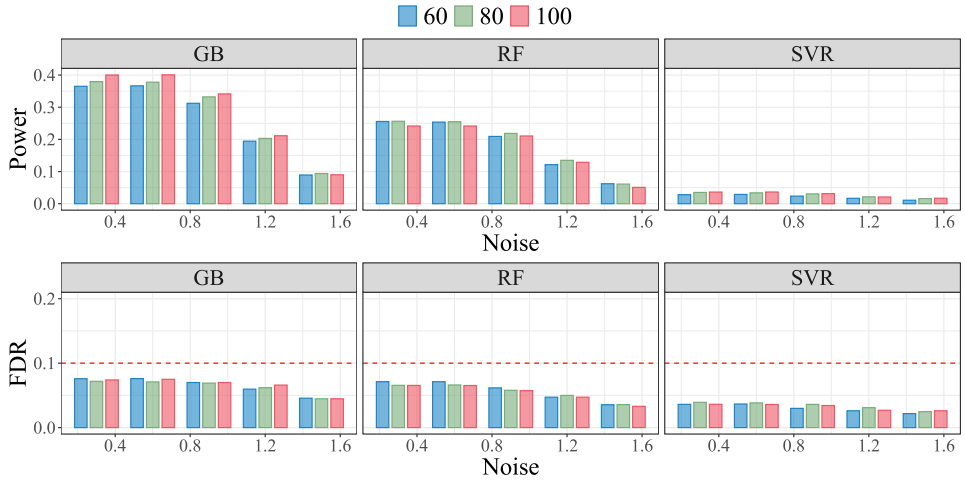


Figure 27: Realized power (left) and FDR (right) of ACS with 200 labeled samples and $k \in \{60, 80, 100\}$ under simulation Setting 1. The other details are the same as in Figure 4.

(`Self_Eval`), or `P(True)`, is the model's own evaluation for the generated answer, which is obtained using the same prompt in Kadavath et al. (2022) as follows:

```
[story]
Question: [question]
Here are some brainstormed ideas: [few_shots examples]
Possible Answer: [generated answer] Is the possible answer:
(A) True
(B) False
The possible answer is: (
```

The self-evaluation score is then defined as the output probability associated with the generated answer "`A)`".

- Input uncertainty scores (Kuhn et al., 2023; Lin et al., 2023). To quantify the uncertainty—or difficulty—of an input, Kuhn et al. (2023) proposed generating M outputs for each prompt. If the responses are consistent, the input is considered less uncertain; conversely, high variability in the generated answers indicates greater uncertainty. Specifically, the selected features include lexical similarity (`Lexical_Sim`), measured by the `rouge-L` score between generated answers. To capture semantic variation, we apply a natural language inference (NLI) classifier to group the M answers into semantically consistent clusters, from which we derive two features: the number of semantic groups (`Num_Sets`) and the semantic entropy (`SE`). Consistent with Kuhn et al. (2023); Lin et al. (2023), we employ a pre-trained DeBERTa-large model (`?`) as the NLI predictor.
- Output confidence scores (Lin et al., 2023; Gui et al., 2024). High likelihoods assigned by large language models (LLMs) do not necessarily correspond to high-quality outputs, as these likelihoods can be poorly calibrated (Zhao et al., 2021; Xiong et al., 2023). To address this issue, Lin et al. (2023) introduced confidence measures derived from the structural similarity among M generated outputs. These measures include the eigenvalues of the graph Laplacian (`EigV`), the average pairwise distances computed via the degree matrix (`Deg`), and the eccentricity (`Ecc`), which incorporates embedding information from each generation. Each metric is computed with respect to a defined similarity function. Following the notation in Lin et al. (2023), we append suffixes `J`, `E`, and `C` to indicate the use of Jaccard similarity, NLI-based entailment scores, and NLI-based contradiction scores, respectively.

With the aforementioned scores, the covariates $\tilde{X}_j$ for question answering tasks is a 13-dimensional vector consisting of `Self_Eval`, `Lexical_Sim`, `Num_Sets`, `SE`, `EigV(C/E/J)`, `Ecc(C/E/J)`, and `Deg(C/E/J)`. In the X-ray report generation task, as the self-evaluation pipeline is not applicable for image inputs, we define $\tilde{X}_j$ as a 12-dimensional vector with remaining scores.

D.1.2 Additional experimental results

As the results with **LLaMA-2-13B-chat** on **CoQA** are presented in Section 6, as a comparison with a different base LLM and a different dataset, we present results with a smaller model **OPT-13B** (Zhang et al., 2023) and results on the **TriviaQA** dataset in this section. The data splitting, ACS, and out-of-sample evaluation pipeline remains the same with Section 6.

CS, ACS, and ACS with new labels incorporation. By fixing $\mathcal{G} \in \{\texttt{logistic}, \texttt{RF}, \texttt{XGBRF}\}$, Experimental results for ACS with new labels (ACS-aug), ACS without label incorporation (ACS), and CS on CoQA and TriviaQA datasets with OPT-13B as the base LLM are presented in Figure 29 and Figure 30. Figure 28 presents the additional results of LLaMA-2-13B-chat on TriviaQA. FDR is controlled for each method for different nominal FDR levels α, but when the nominal level is small, the power of ACS and ACS-aug is much higher than that of CS. Similar to the results with LLaMA-2-13B-chat, the difference in the power of ACS, ACS-aug and CS is even more outstanding with a small sample size and a data-consuming predictive model (e.g., `XGBRF`).

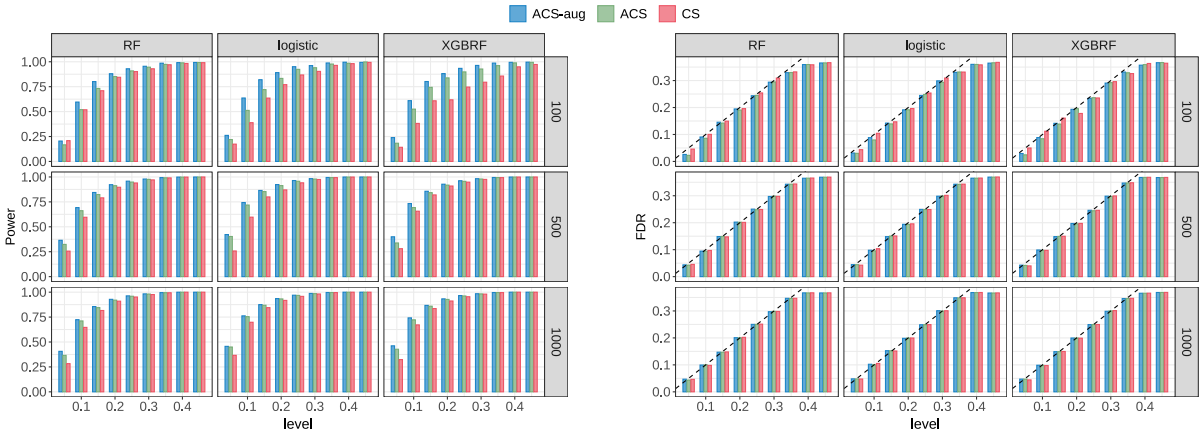


Figure 28: Realized power (left) and FDR (right) of ACS with new labels (ACS-aug), ACS without new labels (ACS), and CS: LLaMA-2-13B-chat + TriviaQA dataset. Details are otherwise the same as Figure 9.

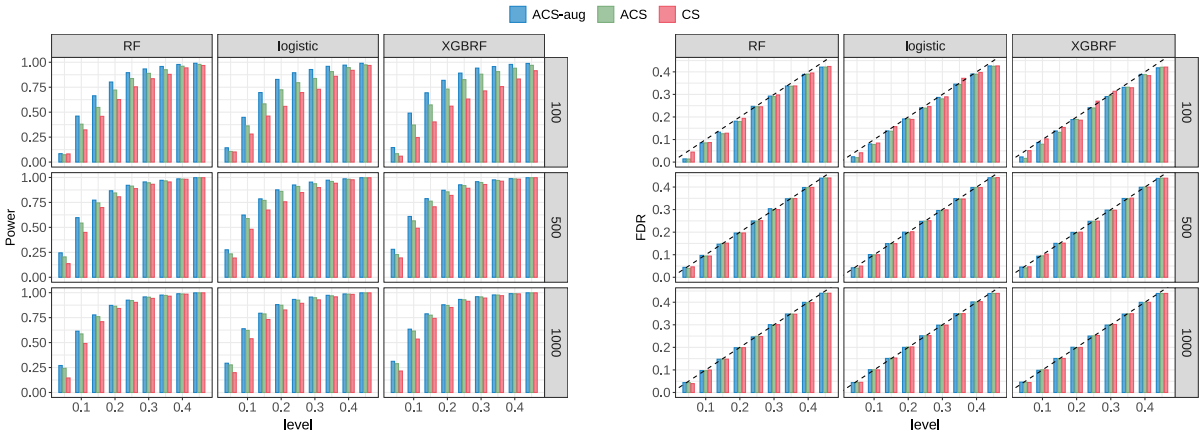


Figure 29: Realized power (left) and FDR (right) of ACS with new labels (ACS-aug), ACS without new labels (ACS), and CS: OPT-13B + CoQA dataset. The target FDR level is $\alpha = 0.1$ and the results are averaged over 200 independent simulations.

ACS with adaptive model selection. Using the same pipeline described in Section 5.3, we compare ACS with adaptive model selection against several baselines: the naive method, CS-logistic, CS-RF, and CS-XGBRF. Figure 31 presents the realized power and FDR with LLaMA-2-13B-chat on TriviaQA, and

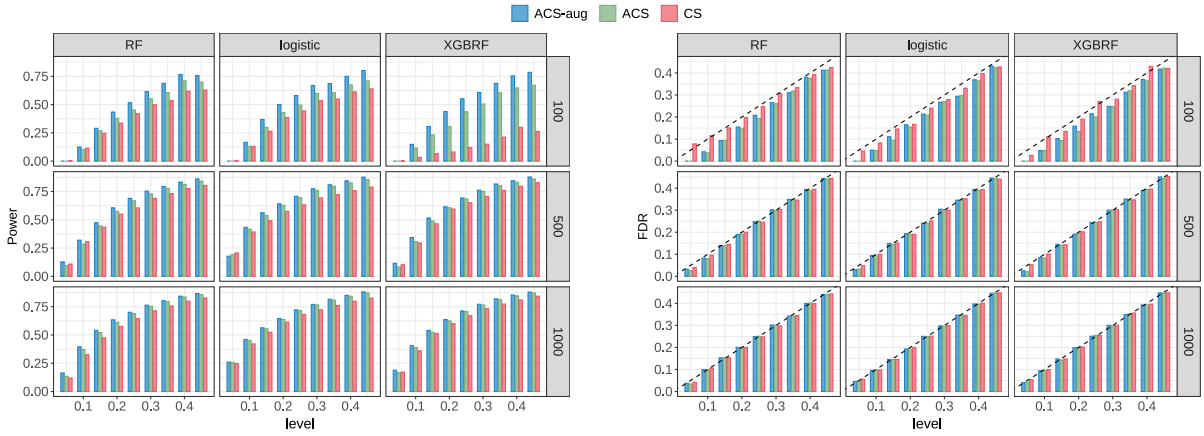


Figure 30: Realized power (left) and FDR (right) of ACS with new labels (ACS-aug), ACS without new labels (ACS), and CS: OPT-13B + TriviaQA dataset. The target FDR level is $\alpha = 0.1$ and the results are averaged over 200 independent simulations.

Figures 32 and 33 report the realized power and FDR of OPT-13B for CoQA and TriviaQA, respectively. Across both datasets, ACS with adaptive model selection consistently achieves the highest power while maintaining FDR control at the target level. This advantage becomes especially evident when the sample size is small or the target FDR level is particularly stringent.

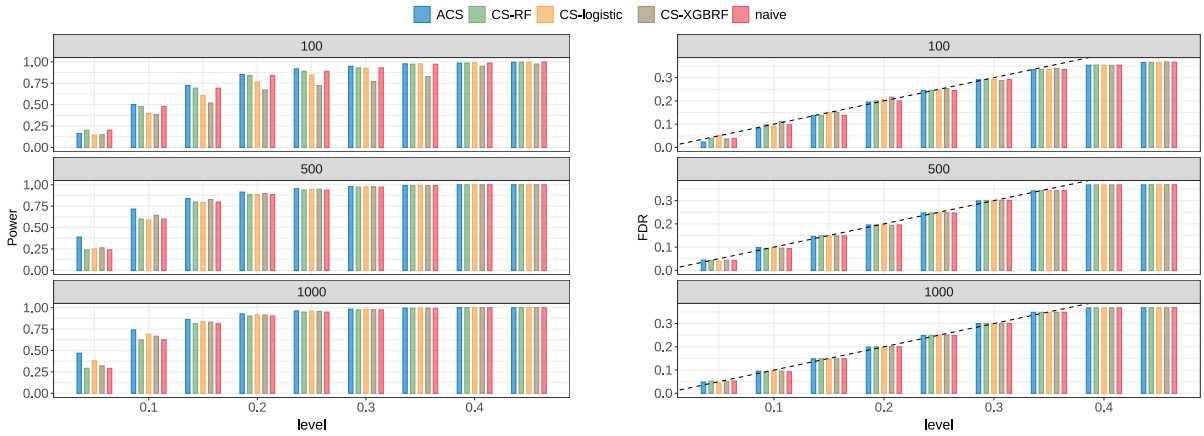


Figure 31: Realized power (left) and FDR (right) of ACS with adaptive model selection, the naive method, CS-SVR, CS-RF, and CS-GB: LLaMA-2-13B-chat + TriviaQA dataset. Each subplot corresponds to the size N of labeled samples. The target FDR level is $\alpha = 0.1$ and the results are averaged over 200 independent simulations.

D.2 Additional drug discovery results

Figure 34 shows the FDR of ACS and CS in the same setting as described in Section 7. Both methods control FDR conservatively.

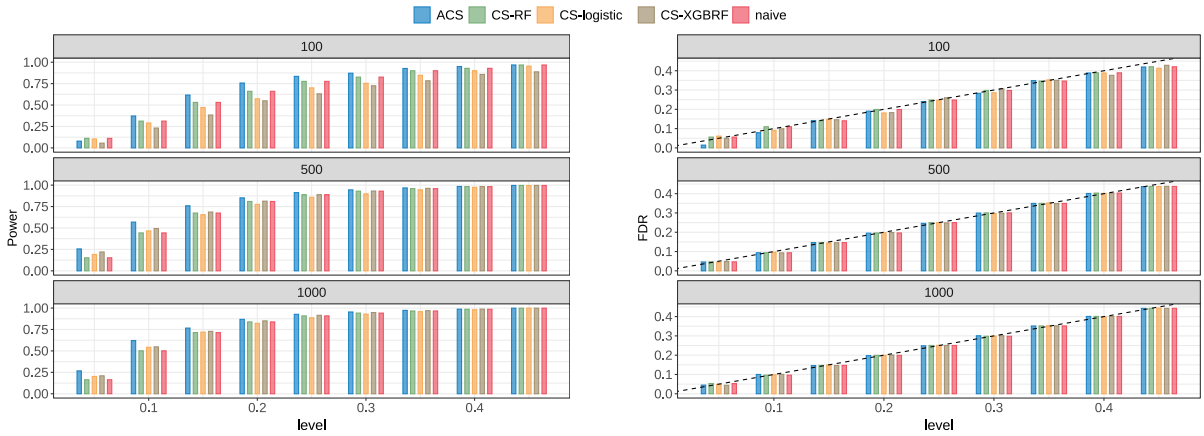


Figure 32: Realized power (left) and FDR (right) of ACS with adaptive model selection, the naive method, CS-SVR, CS-RF, and CS-GB: OPT-13B + CoQA dataset. The target FDR level is $\alpha = 0.1$ and the results are averaged over 200 independent simulations.

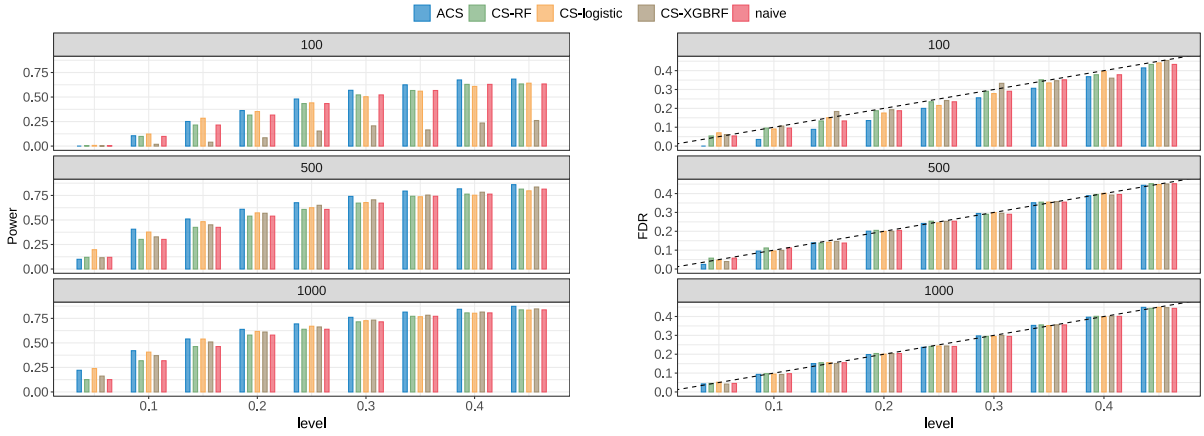


Figure 33: Realized power (left) and FDR (right) of ACS with adaptive model selection, the naive method, CS-SVR, CS-RF, and CS-GB: OPT-13B + TriviaQA dataset. The target FDR level is $\alpha = 0.1$ and the results are averaged over 200 independent simulations.

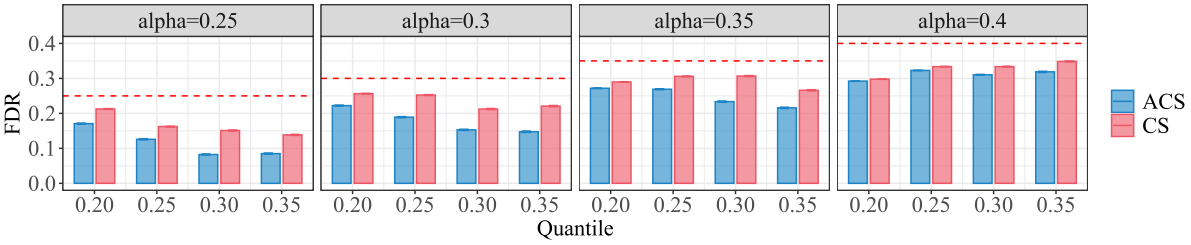


Figure 34: FDR of ACS (blue) compared to CS (red) for various quantile values q and nominal FDR levels α on real drug discovery dataset. Horizontal lines denote the nominal level α.